# Copyright Warning & Restrictions

The copyright law of the United States (Title 17, United States Code) governs the making of photocopies or other reproductions of copyrighted material.

Under certain conditions specified in the law, libraries and archives are authorized to furnish a photocopy or other reproduction. One of these specified conditions is that the photocopy or reproduction is not to be "used for any purpose other than private study, scholarship, or research." If a, user makes a request for, or later uses, a photocopy or reproduction for purposes in excess of "fair use" that user may be liable for copyright infringement,

This institution reserves the right to refuse to accept a copying order if, in its judgment, fulfillment of the order would involve violation of copyright law.

Please Note: The author retains the copyright while the New Jersey Institute of Technology reserves the right to distribute this thesis or dissertation

Printing note: If you do not wish to print this page, then select "Pages from: first page # to: last page #" on the print dialog screen

NJIT New Jersey's Science & Technology University

The Van Houten library has removed some of the personal information and all signatures from the approval page and biographical sketches of theses and dissertations in order to protect the identity of NJIT graduates and faculty.

# ABSTRACT

## RESIDUAL STRESS ANALYSIS OF SPUTTERED TANTALUM SILICIDE THIN FILM

by
Young Joo Song

The influence of different argon pressures on the residual stress, microstructure, and resisitivity of sputtered tantalum silicide thin films has been investigated. $TaSi_2$ films were deposited onto Si wafers by dc magnetron sputtering. The deposition temperature was assumed to be 300°C. The thickness was about 0.5μm. The residual stresses in the films deposited at different argon pressures were determined by curvature measurement method. The compressive intrinsic stress of 1033.4MPa was measured at $P_{Ar}$ = 0.5 mTorr. The intrinsic stress in the films seemed to change from compression to tension as $P_{Ar}$ increased above 8mTorr. A maximum tensile intrinsic stress of 221MPa was obtained at 10 mTorr and the tensile intrinsic stress decreased at the higher argon pressure. SEM showed an accompanying microstructural change from a dense structure at the low pressures to an open growth structure with some gaps between grains at the highest pressure. The electrical resistivity exhibited a sputtering-pressure dependence and seemed to be closely related to the microstructure of films.

# RESIDUAL STRESS ANALYSIS OF SPUTTERED TANTALUM SILICIDE THIN FILM

by
Young Joo Song

A Thesis
Submitted to the Faculty of
New Jersey Institute of Technology
in Partial Fulfillment of the Requirements for the Degree of
Master of Science in Electrical Engineering

Department of Electrical and Computer Engineering

October 1996

## APPROVAL PAGE

## RESIDUAL STRESS ANALYSIS OF SPUTTERED TANTALUM SILICIDE THIN FILM

**Young Joo Song**

---

Dr. Kenneth Sohn, Thesis Advisor — Date
Professor of Electrical and Computer Engineering, NJIT

---

Dr. Roy Cornely, Committee Member — Date
Professor of Electrical and Computer Engineering, NJIT

---

Dr. Robert Marcus, Committee Member — Date
Research Professor of Electrical and Computer Engineering, NJIT

## BIOGRAPHICAL SKETCH

**Author:** Young Joo Song

**Degree:** Master of Science

**Date:** October 1996

**Undergraduate and Graduate Education:**

- Master of Science in Electrical Engineering
  New Jersey Institute of Technology, Newark, NJ, 1996

- Bachelor of Science in Electronic Engineering
  Sogang University, Seoul, Korea, 1993

**Major:** Electrical Engineering

This thesis is dedicated to
Mijoeng and Grace

## ACKNOWLEDGEMENT

The author wishes to express his sincere gratitude to his advisor, Professor Kenneth Sohn, for his guidance and financial support. Special thanks to Professor Robert Marcus and Professor Roy Cornely for serving as members of the committee.

The author is grateful to Mr. Michael Grieco, a manager of NJIT's Microelectronics Research Center (NJIT MRC) for allowing me to use facilities in the cleanroom. The author also wishes to thank Professor James Grow for his help in measurements.

## TABLE OF CONTENTS

## TABLE OF CONTENTS
(Continued)

# LIST OF TABLES

## LIST OF FIGURES

## LIST OF FIGURES
(Continued)

# CHAPTER 1

## INTRODUCTION

Micromechanical sensors are devices which measure physical quantities such as force, pressure, and acceleration through the deformation and/or resulting stresses in suitably designed microstructures. Most silicon based sensors are fabricated from silicon substrates using thin film deposition, patterning, and selective etching of films. However, since these films are often subjected to large mechanical stresses resulting from the specific deposition conditions, temperature changes during processing and in service, and from the presence of passivation coating, there has now developed a strong appreciation that an understanding of mechanical properties is essential for improving the reliability and life time of thin films. Thus, it has become progressively more important to understand the non-electrical properties of thin film materials for use in actuators, sensors, and even VLSI devices.

Recently, the examination of residual stresses in thin films has progressed to the study of the mechanical properties of microelectronic structures and a broad range of thin film materials [1]. These residual stresses cause great problems in not only the fabrication of micromechanical devices, such as wrinkling in thin diaphrams and deflection in cantilevers but also the fabrication of VLSI devices, such as pattern deformation, passivation crack and chip fracture. In these applications, the prediction and the control of stresses are critical because they affect the performance of the devices and even their feasibilities.

The goal of this work is to investigate the residual stresses in sputtered $TaSi_2$ thin films. Since it has been known that the magnetron-sputtered thin films display a rich variety of effects, including compressive-to-tensile stress transitions

as a function of a working gas pressure [2], $TaSi_2$ thin films were deposited on Si substrates at various Ar pressures (deposition from magnetron sources gives access to a wide range of low working gas pressures with minimal substrate heating). After deposition, the residual stresses in the films were measured by curvature measurement method. Finally, SEM micrographs of the films will show that residual stresses correlate directly with microstructural features and physical properties.

Tantalum silicide thin film was chosen as a specimen for several reasons. It is a low resistance material compared to polysilicon (approximately an order of magnitude lower). It has a very high electromigration activation energy, which is 1.7 eV [3] (this is almost three times higher than aluminum of which electromigration activation energy is about 0.6 eV), and this eliminates the reliability problem caused by electromigration. Tantalum silicide is compatible with standard IC processing techniques. In addition, the microhardness of $TaSi_2$ is significantly higher than that of many other silicides.

Chapter 2 describes a fundamental of residual stress in thin films. The origins and types of stresses are investigated and a quantitive calculation of film stress, Stoney formula, is introduced. Finally, the several technologies for stress measurement are discussed.

Chapter 3 examines the properties of tantalum silicide. For this, section 3.1 describes an overview of metal silicides including the reason why the metal silicides have been getting attention of scientists for both VLSI and micromechanical applications. Section 3.2 introduces the methods of formation of silicides and section 3.6 illustrates the properties of tantalum silicide.

Chapter 4 explains the properties of a magnetron sputtering and the microstructure of sputtered films. In section 4.3, an overview of the stresses in magnetron-sputtered thin film is also presented.

Chapter 5 describes the experimental procedures, such as sputter-deposition and stress measurements in detail. In chapter 6, the experimental results, discussions, and challenges are presented. Finally, chapter 7 gives a conclusion of the thesis.

All sputtering depositions were performed at the NJIT Microelectronics Research Center (NJIT MRC) and all measurements were done at NJIT's Thin Film Characterization Lab and NJIT's Optical Imaging Lab.

# CHAPTER 2

# FUNDAMENTALS OF RESIDUAL STRESSES IN THIN FILMS

## 2.1 Origins of Thin Film Stresses

In addition to externally applied stresses, incidential stresses induced during the manufacturing process and during use play significant role in determining the mechanical behavior of thin films. Changes in important physical and chemical properties of the films, adhesion failure, and cracking of the film or substrate may be caused by internal film stress. Some of these negative effects are exaggerated when the film is subjected to additional external loading, particulary when the substrate is flexible or the film is largely unsupported.

Vacuum deposition of thin film on substrates almost always results in internal film stresses, which fall into two basic categories ; thermal and intrinsic stress. Thermal stresses are due to a mismatch of thermal expansion coefficients between film and substrate, and intrinsic stresses are the result of defects accumulated during deposition or growth. Thermal stresses usually develop in thin films when high temperature deposition or high temperature annealing are involved, and are usually unavoidable. To see how mismatch of film and substrate thermal expansion ceofficients generates film stresses, imagine a semi-infinite film deposited on semi-infinite substrate at high temperature. The film is several orders of magnitude thinner than the substrate (the thin film approximation). At this temperature, the thin film is in a stress-free state. Next, imagine detaching the film from the substrate and cooling the system to room temperature (Figure 2.1). Usually, the substrate dimensions undergo minor shrinkage in the plane while the film dimensions are more greatly reduced. In order to reapply the film to the substrate with complete surface coverage, the film must be stretched with a biaxial

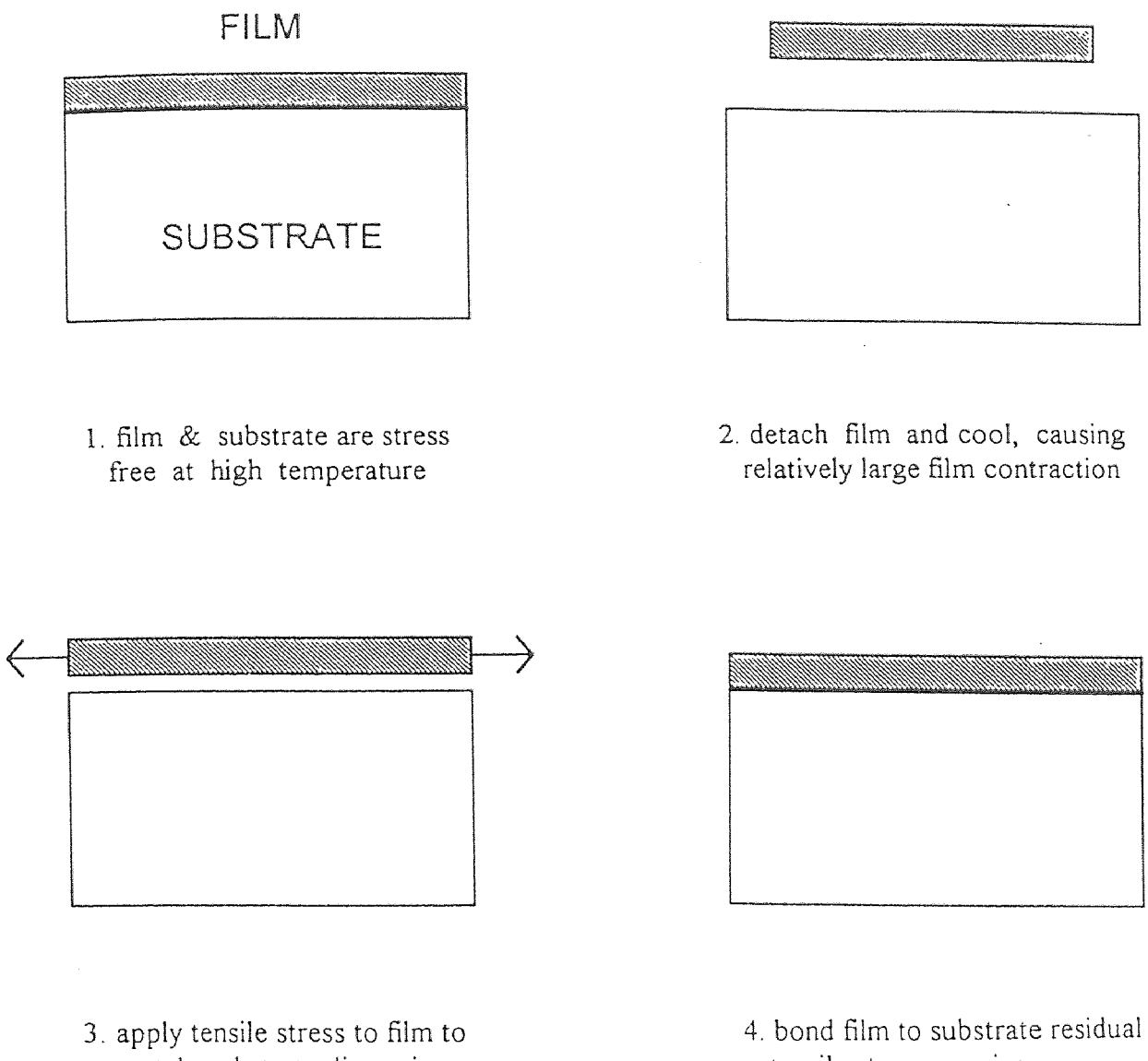


**Figure 2.1** Thermally induced biaxial stress in a thin film

tensile load. This " thought experiment " is analogous to the development of tensile thermal stresses in thin film attatched to substrate.

Intrinsic stresses are due to structural or compositional changes that result in film volume changes. Densification may be due to phase transformation, precipitation, dislocation movement, excess vacancy annihilation, and grain boundary relaxation. Film are sometimes far from thermodynamic equilibrium during deposition. Densification results in stresses that are present in the absence of thermal effects (Figure 2.2). Epitaxial growth stresses may also be present, the result of slight lattice mismatch between film and substrate.

Residual stresses must be superimposed on thermal and intrinsic stresses caused by assembly and normal operation of microelectronic devices. Sensors and actuators are intentionally subjected to additional thermal and mechanical loading in the performance of the functions for which they were designed. Also, particulary in soft and low melting point materials like aluminum, residual stresses tend to relax through diffusion. Flaws such as voids and hillocks may form, creating weak points where failure is likely. Thus, an understanding of all sources of stress is critical for complete understanding of thin film mechanical properties (Figure 2.3).

## 2.2 Tensile and Compressive Stress in Film

Thin films can be stressed even without the application of external loading and are said to possess residual stresses. Residual stresses are, of course, not restricted to composite film-substrate structures, but occur universally in all classes of homogeneous materials under special circumstances. A state of nonuniform plastic deformation is required, and this frequently occurs during mechanical or thermal processing. For example, when a metal strip is reduced slightly by rolling between cylindrical rolls, the surface fibers are extended more than the interior bulk.

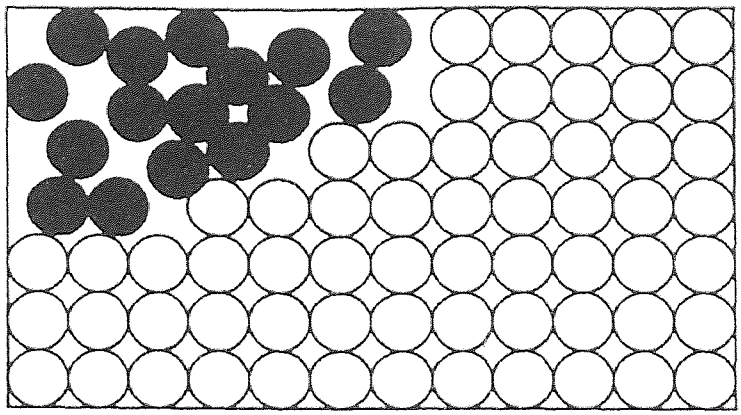

Grains 1 and 2 before growth. Atoms in grain #1 are heavily shaded.

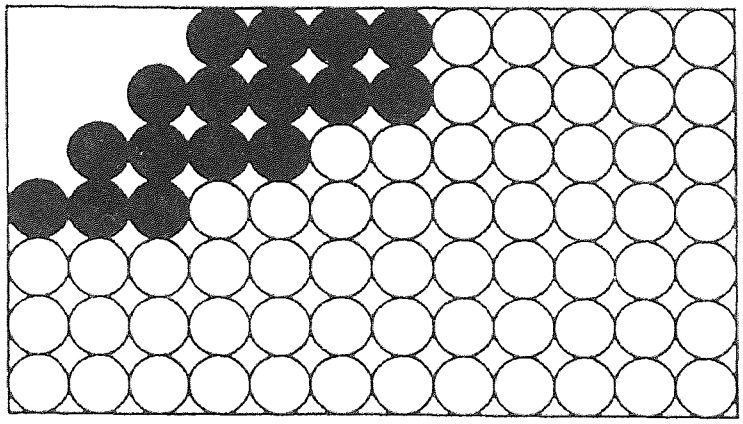

Growth of grain #1 has caused a volume change. The film must have tensile stress

**Figure 2.2** Grain growth induced stress in a thin film

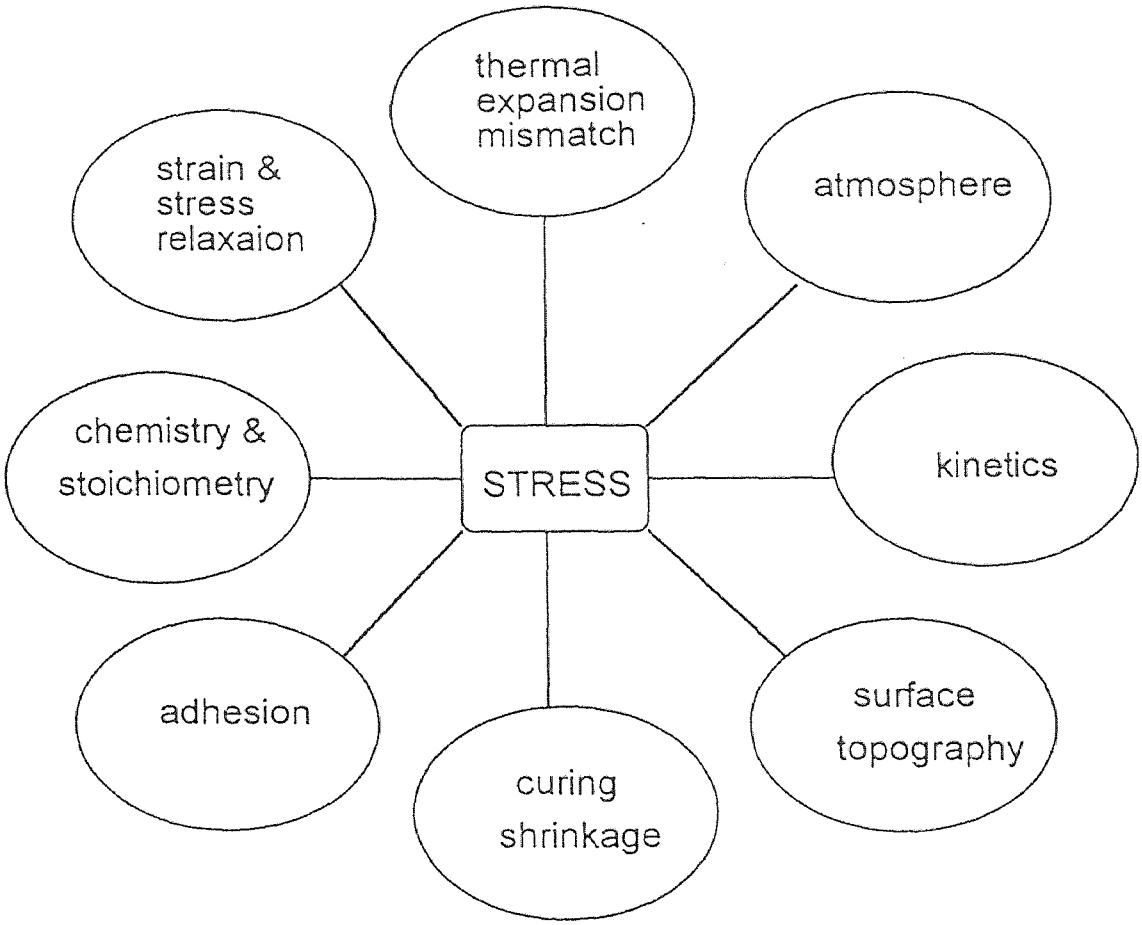


**Figure 2.3** Parameters that affect thin film stress [4]

Machining a thin surface layer from the rolled metal will upset the mechanical equilibrium and cause the remaining material to bow.

Residual stresses arise in casting, welds, machined and ground materials, and heat-treated glass. The presence of residual stresses is usually undesirable, but there are cases where they are benefical. Tempered glass and spot-peened metal surfaces rely on residual compressive stresses to counteract harmful tensile stresses applied in service. A model for generation of residual stress during the deposition of films is illustrated in Figure 2.4. Regardless of the stress distribution that prevails, maintenance of mechanical equilibrium requires that the net force $F$ and bending moment $M$ vanish on the film-substrate cross section. Thus,

$$F = \int \sigma dA = 0 \tag{2.1}$$

$$M = \int \sigma y dA = 0 \tag{2.2}$$

where $A$ is the sectional area and $y$ is the moment lever arm. Intuitive use will be made of these basic equations, and they are applied analytically in deriving the Stoney formula in the next section. In the first type of behavior shown in Figure 2.4 (a), the growing film initially shrinks relative to the substrate. Surface tension forces are one reason why this might happen ; the misfit accompanying epitaxial growth is another. Compatibility, however, requires that both the film and substrate have the same length. Therefore. the film is constrained and stretches, and the substrate accordingly contracts. The tensile forces developed in the film are balanced by the compressive forces in the substrate.

However, the combination is still not in mechanical equilibrium because of the uncompensated end moments. If the film-substrate pair is not restrained from moving, it will elastically bend as shown, to counteract the unbalanced moments.

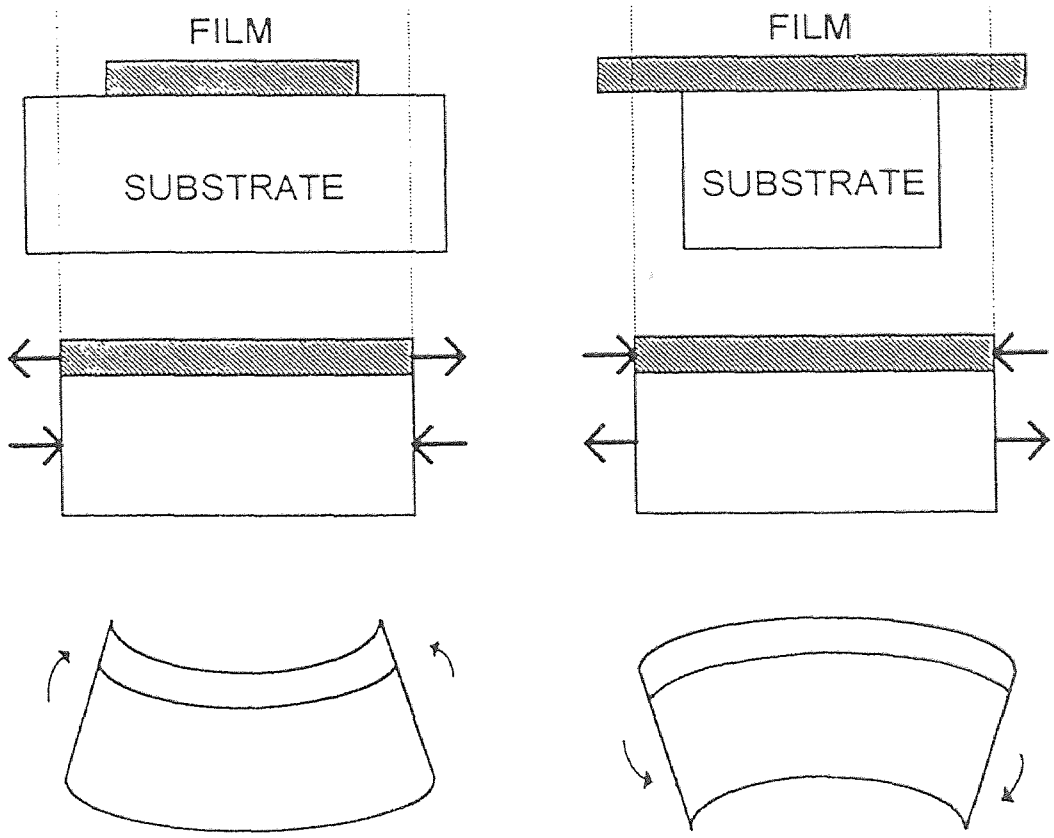


(a) Film under residual tensile stress

(b) Film under residual compressive stress

**Figure 2.4** Sequence of events leading to (a) residual tensile stress in film ; (b) residual compressive stress in film

Thus, films containing residual tensile stresses bend the substrate concavely upward. In an entirely similar fashion, compressive stresses develop in films that tend to initially expand relative to substrate (Figure 2.4 (b)). Residual compressive film stresses, therefore, bend the substrate convexly outward. These relations are perfectly general regardless of the specific mechanisms that cause films to stretch or shrink relative to substrates. Sometimes the tensile stresses are sufficiently large to cause film fracture. Similarly, excessive high compressive stresses can cause film wrinkling and local loss of adhesion to the substrate.

## 2.3 The Stoney Formula

We now turn our attention to a quantitative calculation of film stress as a function of substrate bending. The formulas that have been used in virtually all experimental determinations of film stress are variants of an equation first given by Stoney in 1909 [5]. This equation can be derived with reference to Figure 2.5, which shows a composite film-substrate combination of width $w$. The film thickness and Young's modulus are $d_f$ and $E_f$, respectively, and the corresponding substarte values are $d_s$ and $E_s$. Due to lattice misfit, differential thermal expansion, film growth effects, etc., mismatch forces arise at film-substrate interface. In the free-body diagrams of Figure 2.5 (b) each set of interfacial forces can be replaced by the statically equivalent combination of a force and moment : $F_f$ and $M_f$ in the film, $F_s$ and $M_s$ in the substrate, where $F_f = F_s$. Force $F_f$ can be imagined to act uniformly over the film cross section ($d_f w$) giving rise to the film stress. The moments are responsible for the bowing of the film-substrate composite. Equation (2.2) requires equality of the clockwise and counterclockwise moments, a condition expressed by

$$(( d_f + d_s ) / 2 ) F_f = M_f + M_s \qquad (2.3)$$

Consider now an isolated beam bent by moment $M$, as indicated in Figure 2.5 (c). In this case, the deformation is assumed to consist entirely of the extension or contraction of longitudinal beam fibers by an amount proportional to their distance from the central or neutral axis, which remains unstrained in the process. The stress distribution reflects this by varying linealy across the section from maximum tension ( $+\sigma_m$ ) to maximum compression ( $-\sigma_m$ ) at the outer beam fibers. In terms of the beam radius of curvature $R$, and angle $\theta$ subtended, Hooke's law yields

$$\sigma m = E \left\{ \frac{(R \pm d/2)\,\theta - R\theta}{R\theta} \right\} = \pm \frac{E\,d}{2\,R} \qquad (2.4)$$

Corresponding to this stress distribution is the bending moment across the beam section :

$$M = 2 \int_0^{d/2} \sigma_n\, w \left( \frac{y}{d/2} \right) y dy = \frac{\sigma_n d^2 w}{6} = \frac{E\,d^3 w}{12R} \qquad (2.5)$$

By extention of this result, we have

$$M_f = E_f d_f^2 w / 12\,R \quad \text{and} \quad M_s = E_s d_s^3 w / 12\,R \qquad (2.6)$$

Lastly, in order to account for biaxial stress conditions, it is necessary to replace $E_f$ by $E_f / (1 - \nu_f)$, and similarly for $E_s$. Substitution of these terms in Equation (2. 3) yields

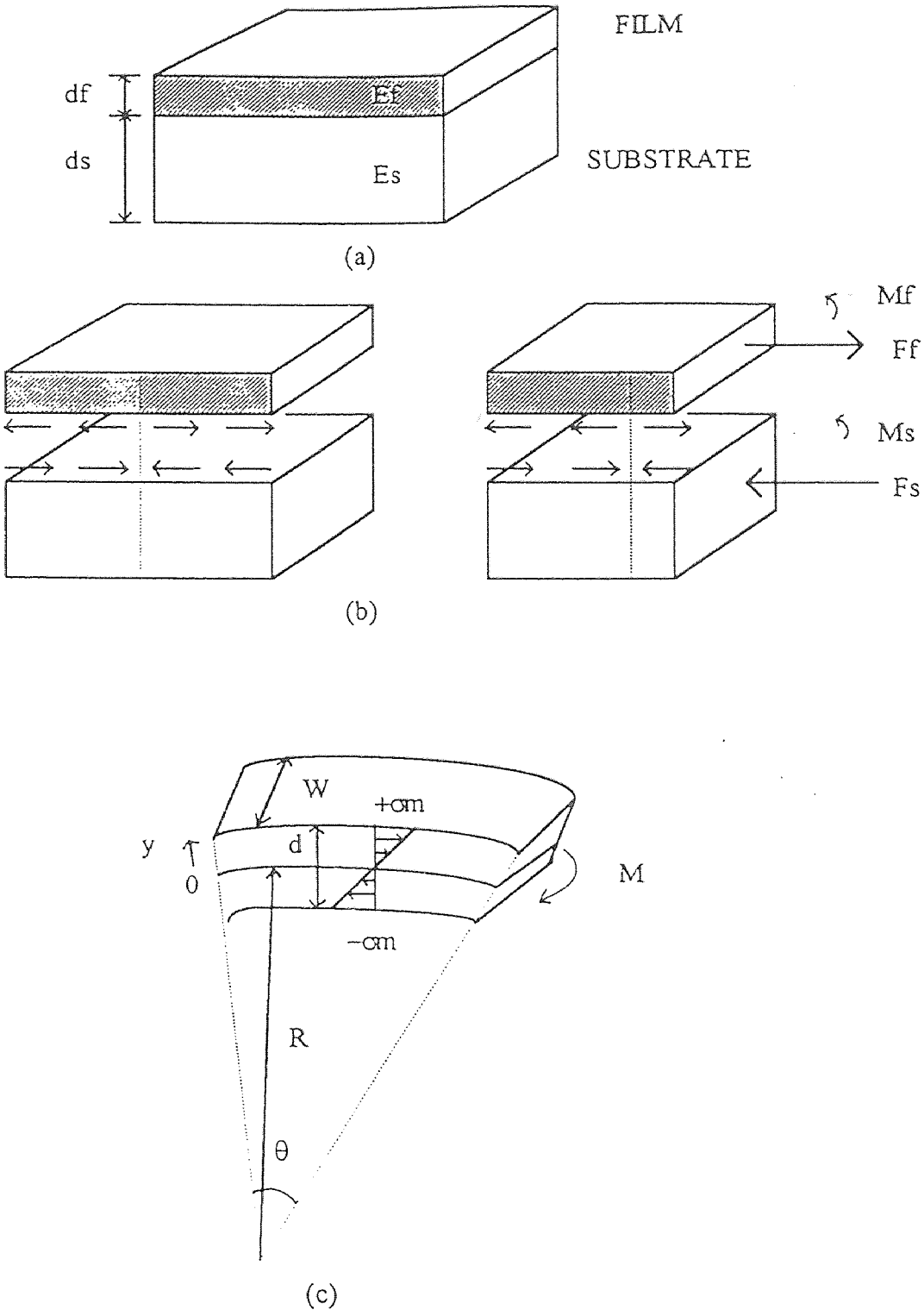


**Figure 2.5** Stress analysis of film-substrate combination ; (a) composite structure (b) free-body diagrams of the film and substrate with indicated interfacial forces and end moments (c) elastic bending of beam under applied end moment

$$\left(\frac{df + ds}{2}\right) Ff = \frac{w}{12R}\left[\left(\frac{Ef}{1 - vf}\right) df^3 + \left(\frac{Es}{1 - vs}\right) ds^3\right] \qquad (2.7)$$

Since $d_s$ is normally much larger than $d_f$, the film stress $\sigma_f$ is, to a good approximation, given by

$$\sigma_f = \frac{Ef}{df\, w} = \frac{1}{6R} \cdot \frac{Es\, ds^2}{(1 - vs)\, df} \qquad (2.8)$$

Equation (2.8) is the Stoney formula. Values of $\sigma_f$ is are determined through measurement of $R$.

## 2.4 Stress Measurement Techniques

Three basic methods exist for measuring the stresses of the thin films on the substrates : curvature measurement, x-ray diffraction, and photoelastic method.

### 2.4.1 Curvature (Bending) Measurement Method

Curvature measurement is based on bending forces exerted by thin films on substrate. This method is used for both in-situ and post-processing measurements of residual stresses. Several mechanical property measuring methods are also based on this effect. A biaxial stress in a thin film on a substrate will cause the substrate to elastically deform. The biaxial stress produces shear stresses on the film / substrate interface near the edges of the film. Bending deformation is due to these shear stresses. If the thin-film approximation is made, only the biaxial modulus of the substrate must be considered in evaluating the bending due to biaxial stresses. No thin film properties must be assumed. Film stress is directly proportional to displacement.

For in-situ measurement of the film stresses during film deposition, cantilever beams are commonly employed [6]. Beam-tip deflection can be measured by a variety of techniques. In-situ measurement is complicated by the need to consider other bending mechanisms such as momentum transfer from the deposition process [7] and temperature gradients [8]. After deposition, secondary bending sources no longer require consideration, but complications arise from geometric deviations from beam theory found in microcantilever beams.

A disc-shaped substrate is most often used for post-processing stress measurements. This technique measures average biaxial stress in a film over a relatively large area and avoids some of the geometric complications of microcantilever measurements. Optical measurement methods such as interferometry and laser rastering, and grazing incidence x-ray scattering (GIXS) techniques are used.

Interferometry determines curvature from the interference between reflections from the substrate and a flat surface [9]. Laser rastering measures the deflection of a laser beam reflected from the substrate surface [10] (Figure 2.6). These methods measure average stress in plane and through thickness through the properly designed equipments.

### 2.4.2 X-Ray Diffraction Method

When a polycrystalline piece of metal is deformed elastically in such a manner that the strain is uniform over relatively large distances, the lattice plane spacings in the constituent grains change from their stress-free value to some new value corresponding to the magnitude of the applied stress, this new spacing being essentially constant from one grain to another for any particular set of planes similarly oriented with respect to the stress. This uniform microstrain causes a shift of the diffraction lines to new $2\theta$ positions. On the other hand, if the metal is

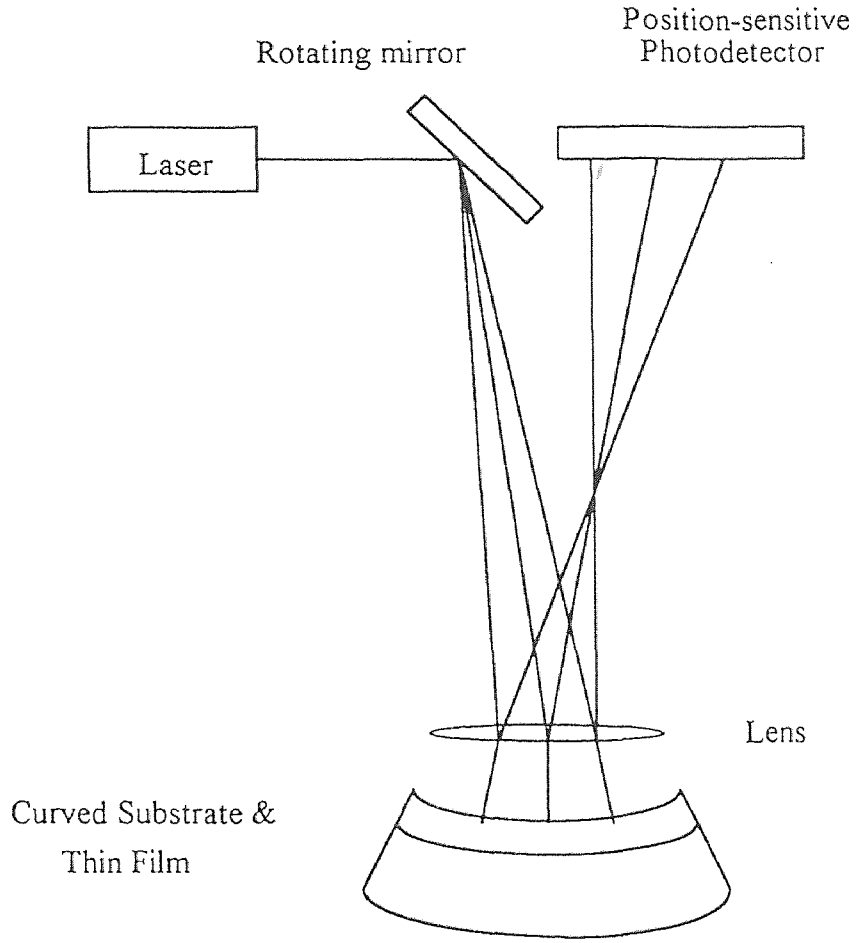


**Figure 2.6** Laser measurement of wafer curvature ; If the sample is warped, the extent of the reflected image is an indication of its radius of curvature

deformed plastically, the lattice planes usually become distorted in such way that the spacing of any particular (*hkl*) set varies from one grain to another or from one part of a grain to another. This nonuniform microstrain causes a broadening of the corresponding diffraction line. Actually, both kinds of strain are usually superimposed in plastically deformed metals, and diffraction lines are both shifted and broadened, because not only do the plane spacings vary from grain to grain but their mean value differs from that of the undeformed metal.

X-ray method is nondestructive for measurement of surface stress. If the stress is to be measured at some point below the surface, material must be removed down to that point to expose a new surface for x-ray examination ; the x-ray method then becomes destructive. Ordinarily, however, one is most interested in the stress at the surface, where the applied stress is usually highest and where failures usually originate.

The x-ray method has the great advantage that it makes possible repeated measurements on the same specimen. For example, we may measure stress before and after some treatments designed to produce or modify various stages in its service life. Note also that the x-ray method measure the existing stress, whether it be solely residual or the sum of residual and applied. It therefore has the capability measuring the actual service stress in a machine or structure under a service load. Note, however, that stress is not measured directly by the x-ray method but by calculation or calibration. In principle, the x-ray method is applicable to any polycrystalline material. While it has had some application to stress measurement in ceramic and rocks, its major use is the measurement of residual stress in metals and alloys.

Since the angular position $2\theta$ of the diffracted beam is meausred directly with a diffractometer, it is convenient to write the stress equation in terms of $2\theta$ rather than plane spacings. Equation (2.9) allows us to calculate the stress in any

chosen direction from plane spacing obtained from two measurements made in a plane normal to the surface and containing the direction of the stress to be measured. (Figure2.7)

$$\sigma_\phi = \frac{E}{(1+\nu)\sin^2\psi}\left(\frac{d_i - d_n}{d_n}\right) \tag{2.9}$$

Differentiating the Bragg's law ( $\lambda = 2\,d\sin\theta$ ), we obtain

$$\frac{\Delta d}{d} = -\frac{\cot\theta\,\Delta 2\theta}{2} \tag{2.10}$$

Combining this relation with Equation (2.9) gives

$$\sigma_\phi = \frac{E\cot\theta\,(2\theta_n - 2\theta_i)}{2\,(1+\nu)\,\sin^2\psi} \tag{2.11}$$

Put

$$K_1 = \frac{E\cot\theta}{2\,(1+\nu)\sin^2\psi} \tag{2.12}$$

Then

$$\sigma_\phi = K_1\,(2\theta_n - 2\theta_i) = K_1\,(\Delta 2\theta) \tag{2.13}$$

where $2\theta_n$ is the observed value (in radians) of the diffractometer angle in the "normal" measurement ($\psi = 0$) and $2\theta_n$ is the value in the inclined measurement ($\psi = \psi$). Figure 2.8 shows the use of diffractometer for stress measurement. the constant $K_1$ is called the stress constant. For greatest sensitivity $K_1$ should be as large as possible.

The x-ray method has been reviewed by Barrett and Massalski [11], Klug

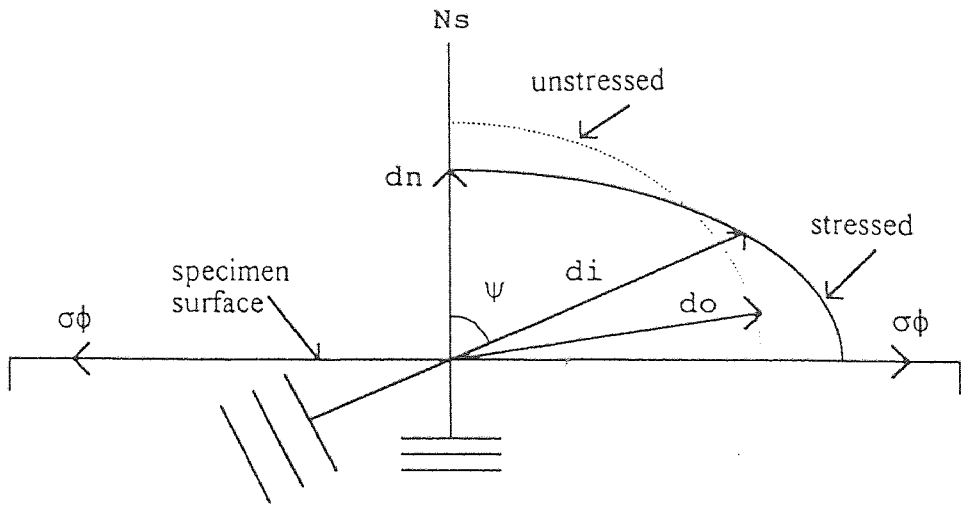


(a) Vector diagram of plane spacings d for a tensile stress σϕ

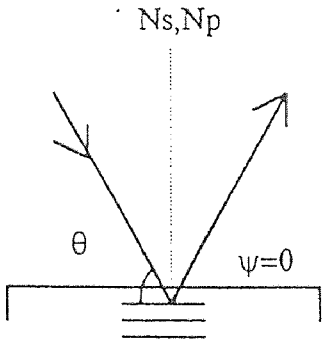


(b) Measurement of dn

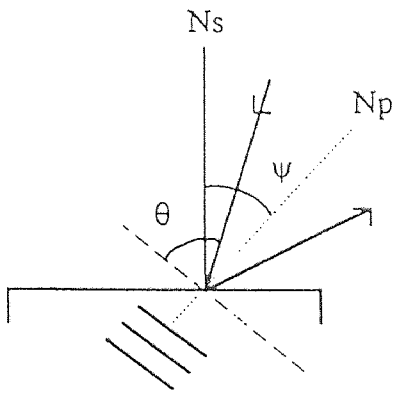


(c) Measurement of di

**Figure 2.7** (a) Plane-spacing diagram ; (b) and (c) Orientations of x-ray beams relative to specimen (Ns = normal to specimen surface, Np = normal to reflecting planes )

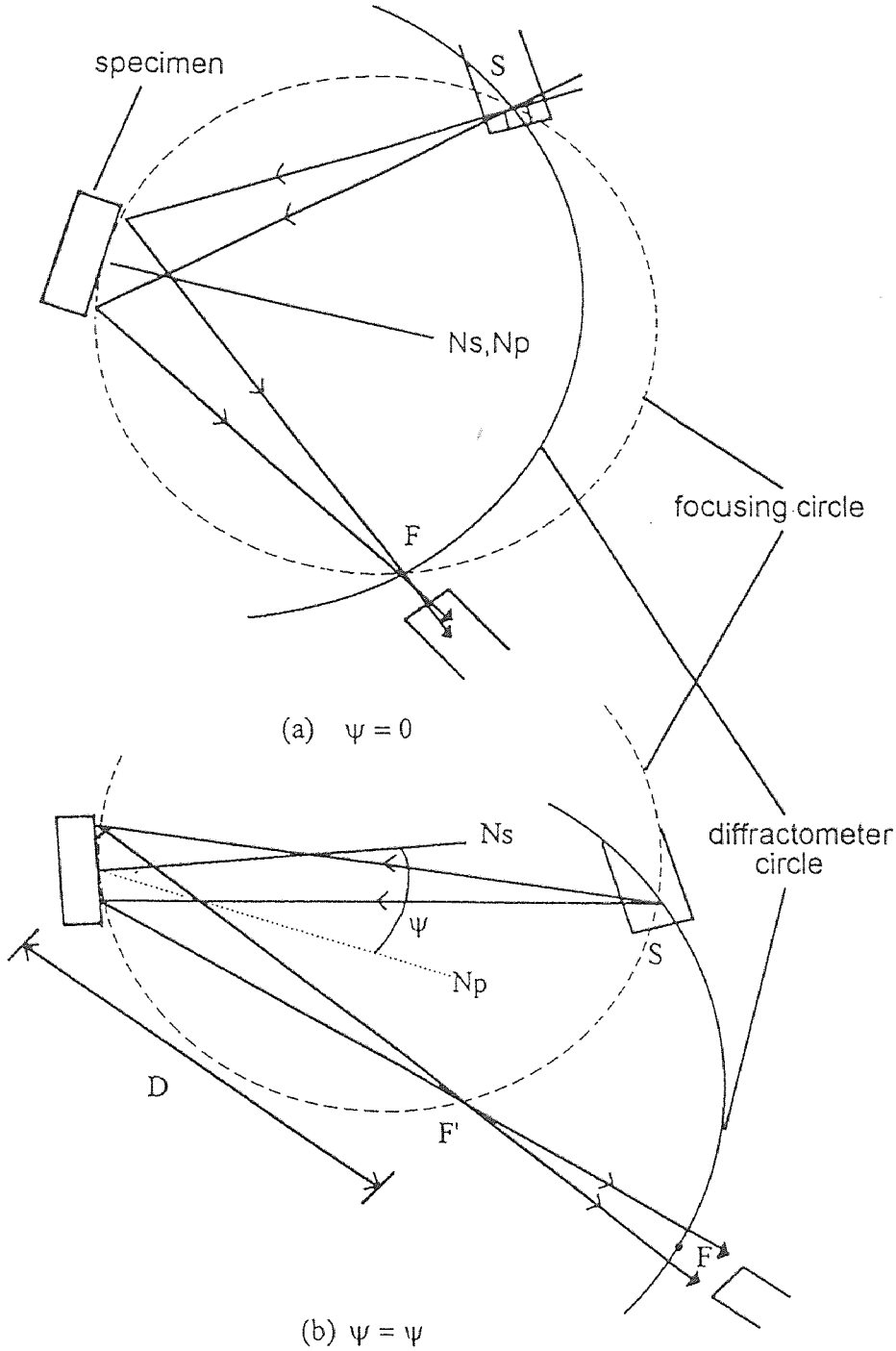


**Figure 2.8** Use of a diffractometer for stress measurement

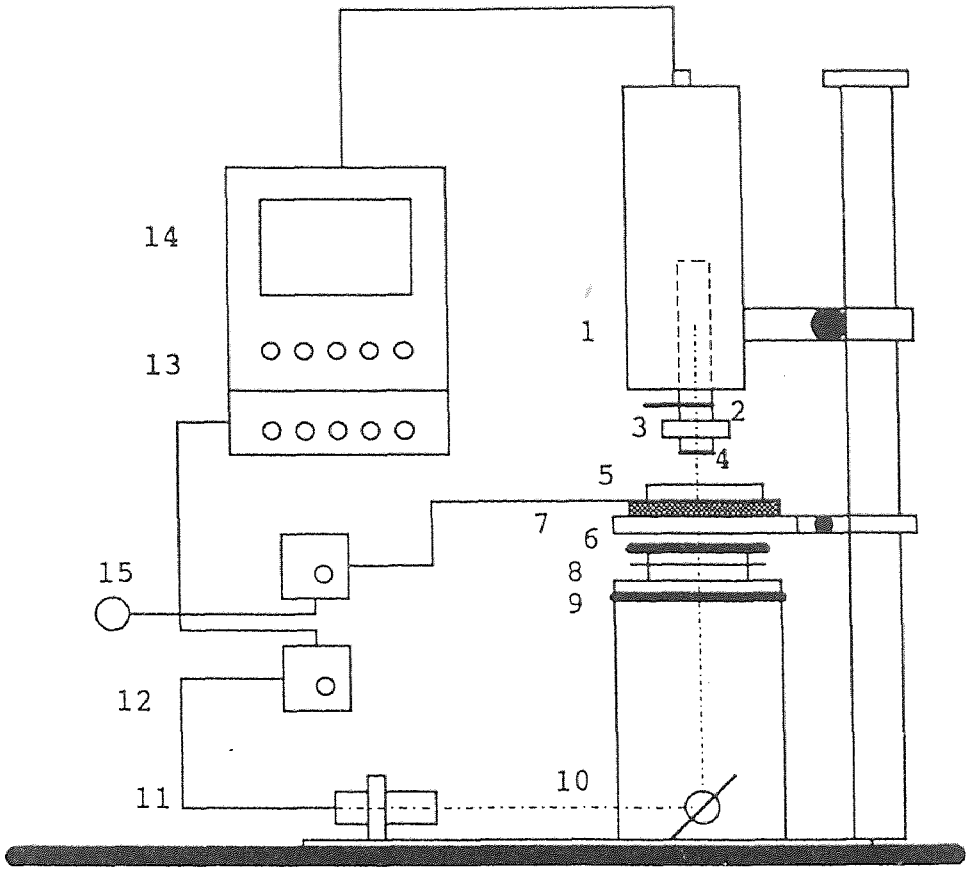


1. IR vidicon camera, 2. IR polarizer, 3. lens, 4. 1/4 wave plate, 5. heating stage, 6. sample, 7. 1/4 wave plate, 8. IR polarizer, 9. condenser, 10. mirror box, 11. light source, 12. light source controller, 13. camera controller, 14. monitor TV, 15. heating stage controller.

**Figure 2.9** Infrared photoelastic apparatus

and Alexander [12], Taylor [13], and Norton [14,15]. A detailed treatment has been published by the Society of Automotive Engineers [16].

### 2.4.3 Photoelastic Method

When a beam of polarized light pases through an elastically stressed sample which consists of transparent isotropic material, the beam decomposed into two rays polarized in the planes of principal stresses in the sample. Therefore, interference patterns will develop which are proportional to the difference in the principal stresses. A setup for the photoelastic measurements are shown in Figure 2.9 [17].

# CHAPTER 3

# INVESTIGATION OF TANTALUM SILICIDE

## 3.1 Background of Silicide

The primary thrust of very large scale integration (VLSI) has been the miniaturization of devices to increase packing density, achieve higher speed and consume less power [18]. The continued evolution of smaller and smaller devices has aroused a renewed interest in the development of new metallization schemes for low resistivity gates, interconnection, and ohmic contacts. This interest in new metallization schemes has been aroused by the fact that with the scaling down of the device sizes, the line width gets narrower and sheet resistance contributing to RC delay increases.

Aluminum and its alloys have been used extensively for metallization in intergrated circuits because of their low resistivities ( i.e., 2.7 $\mu\Omega$-cm for Al and upto 3.5 $\mu\Omega$-cm for its alloys ). However, the use of aluminum in intergrated circuits creates problems, such as junction spiking and electromigration [19] . It is also requires all post gate deposition processing of the devices to be limited to very low temperatures preferably below 500°C. Aluminum on silicon leads to metallurgical interactions causing serious instabilities. Annealing of aluminum on silicon (typically at 450°C) causes dissolution of silicon by diffusion into the metal and leads to pit formation [20]. The pits in silicon become visible after selectively removing Al from the surface. In actual devices, diffused aluminum is present in silicon below the Al / Si interface. If the penetration is deep, it leads to contact and junction failure. Electromigration causes considerable material transports in Al because of the enhanced and directional mobility of atoms caused by electron momentum transfer. Aluminum gathers in the direction of electron flow, leading

to a discontinuity in the current-carrying lines. This type of device failure seriously affects the reliability of silicon devices [21].

Instead of metal, polysilicon can be used as a gate material and/or an interconnection. The structure of polysilicon is strongly influenced by dopants, impurities, deposition temperature and post deposition cycles [22]. Films deposited for temperatures below 575°C, are amorphous with no detectable structure. Polysilicon deposited above 625°C has a columnar structure, which leads to higher resistivity. The undoped polysilicon films can be highly resistive (400-700 Ω-cm). However, their resistivity can be decreased by doping them with appropriate dopant gases introduced during the deposition process. The major disadvantage of polysilicon as a gate material is its high resistivity. With the increasing complexity and density of ICs, the width and spacing of the polysilicon runners have to be reduced. With desired improvements in speed-power product, the RC delay introduced by the polysilicon films becomes unacceptable.

Refractory metals were investigated for applications in VLSI technology in the 1970's. The two most commonly investigated materials were tungsten and molybdenum [23,24]. These materials have much higher melting points than silicon and their thermal expansion coefficients are similar to that of silicon. But the use of refractory metals requires complete passivation of these metals from oxidizing ambient and they may form silicides at temperatures above 900°C when they are in contact with silicon. The formation of silicides is accompanied by a volume shrinkage which can result in development of cracks. These cracks pose functional and reliability problems in ICs. Among many problems of refractory metals are those of cleanliness, contact to other conductors, and deposition and etching of the metals for pattern generation. The uncertainties associated with the stability of these metal films have led to search for alternative materials.

The silicides have attracted attention because of their low resistivities and

high temperature stability. The use of silicides, with resistivity values one tenth those of polysilicon, is certain to improve the speed of ICs. Expected higher electromigration resistance and the possibility of forming silicides directly on polysilicon, thus preserving the basic polysilicon MOS gate while decreasing the resistance, make these silicides attractive for gate and interconnect metallization [25,26]. Table 3.1 [27] shows the comparison of properties of the silicides of Ti, Ta, Mo, and W.

## 3.2 Formation of Silicide

Silicides can be formed by, basically, four techniques, each of which involve a metal deposition followed by a thermal step to form the silicide :

(1) Direct metallurgical reaction : deposition of the pure metal on silicon (i.e. onto single crystal or polycrystalline silicon)

(2) Co-evaporation : Simultaneous evaporation of the silicon and the refractory metal from two sources

(3) Chemical Vapor Deposition : Formation of a thin film on Si by the reaction of vapor phase chemicals (reactants) that have the required constituents

(4) Sputtering : Sputter deposition of the silicide, either from a composite target, or by cosputtering or layering

### 3.2.1 Direct Metallurgical Reaction

In this technique, a refractory metal film is deposited directly on a silicon surface, and the wafer is annealed at relatively low temperatures. Metal silicides are initially formed and continue to grow until the metal is consumed [28]. Typically at this point, the next metal rich phase begins to grow. For example, Figure 3.1 shows the effect of temperature on the formation of $WSi_2$ and $W_5Si_3$. $W_5Si_3$ has

**Table 3.1** Comparison of the properties of silicides of Ti, Ta, Mo and W

| Property | $TiSi_2$ | $TaSi_2$ | $MoSi_2$ | $WSi_2$ |
|---|---|---|---|---|
| Resistivity ($\mu\ \Omega$-cm) | ≈ 25 | ≈ 50–55 | ≈ 90–100 | ≈ 70 |
| Formed by co-deposition [a] of metal and Si followed by sintering | | | | |
| Etch rate in (10:1)BHF (Å/min) | ≥2000 | 100-300 | small | small |
| Dry etching in | | | | |
| (a) Plasma | Yes | Yes | Yes | Yes |
| (b) RSE | Yes | Yes | Yes | Yes |
| Oxidation in | | | | |
| (a) Dry $O_2$ | Yes | No (Yes)[b] | Yes | Yes |
| (b) Wet $O_2$ | Yes | Yes | Yes | Yes |
| Stability of the metal oxide | Good | Good | Poor, vaporizes | Poor, vaporizes |
| Oxidation Stability of silicide on | | | | |
| (a) silicon | Good | Good | Good | Good |
| (b) oxide | Good | Fair | Poor | Poor |
| Al-silicide interaction temperature (°C) | >500 | >500 | >500 | >500 |
| Recommended for use | | | | |
| (a) on oxide | Yes | Yes[c] | No | No |
| (b) on silicon | Yes | Yes | Yes | Yes |

[a] Cosputtering, sputtering from sintered target or coevaporation

[b] No for Ta sintered on polysilicon to form silicide and yes for cosputtered silicide on polysilicon

[c] Not to be exposed to oxidizing ambients at high temperature

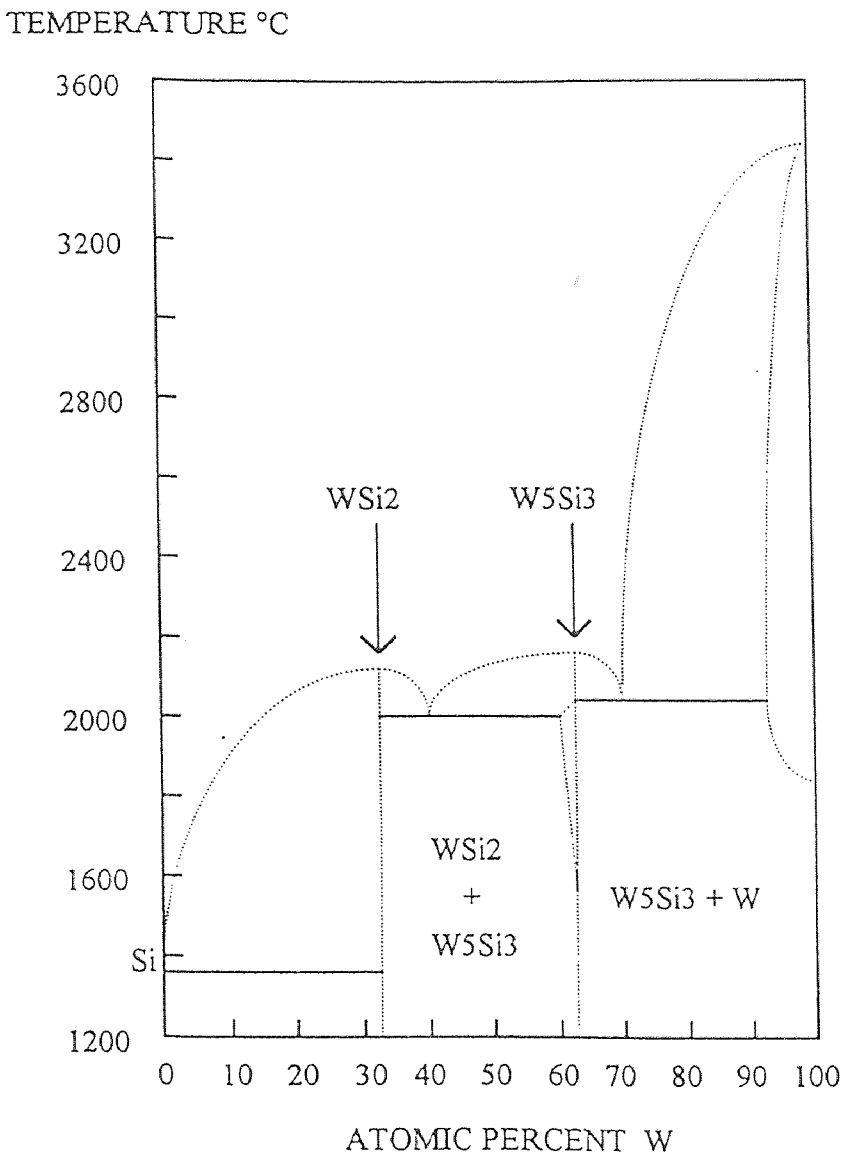


**Figure 3.1** Phase diagram of tungsten-silicon system

has the highest melting point and $WSi_2$ has the least. This temperature dependence has been observed for most silicide formations and is an indication of a diffusion limited process. In this $WSi_2$ reaction, for each angstrom of tungsten thickness consumed, 2.53 Å of silicon are consumed resulting in 2.58Å of $WSi_2$ being formed. An important care must be taken so that the sufficient silicon should be available when using this technique.

### 3.2.2 Co-Evaporation

The evaporation method utilizes the simultaneous of the metal and Si under high vacuum conditions. The metal and Si can be vaporized by electron beam, rf induction, laser, or resistive heating. Since the refractory metals like W, Ta, Ti, and Mo have very high melting points (1670 °C to 2996°C) and silicon has a low vapor pressure, e-beam evaporation can be chosen as a best choice. In e-beam evaporation a stream of electrons is accelerated to high kinetic energy and the beam is directed at the material to be evaporated and the kinetic energy is transformed to thermal energy upon impact. As the material is held at high temperature, this electron stream can melt and evaporate any material provided that the beam can supply an energy to the evaporant at an equal rate at which heat is lost. Electron beam guns are built to supply up to 1200KW of highly concentrated electron beam power for evaporation applications. Very high film deposition rates can thereby be obtained as a result of high power available. Typically two guns are employed with separate power supplies. Careful determination of the evaporation rate as a function of power for both metal and Si must be determined. The correct amount of power is supplied to each gun to provide the proper M/Si ratio, where M denotes metal. X-ray damage from e-beam evaporation is generally annealed out during the high temperature sinter operation. A typical configuration for depostion is shown in Figure 3.2.

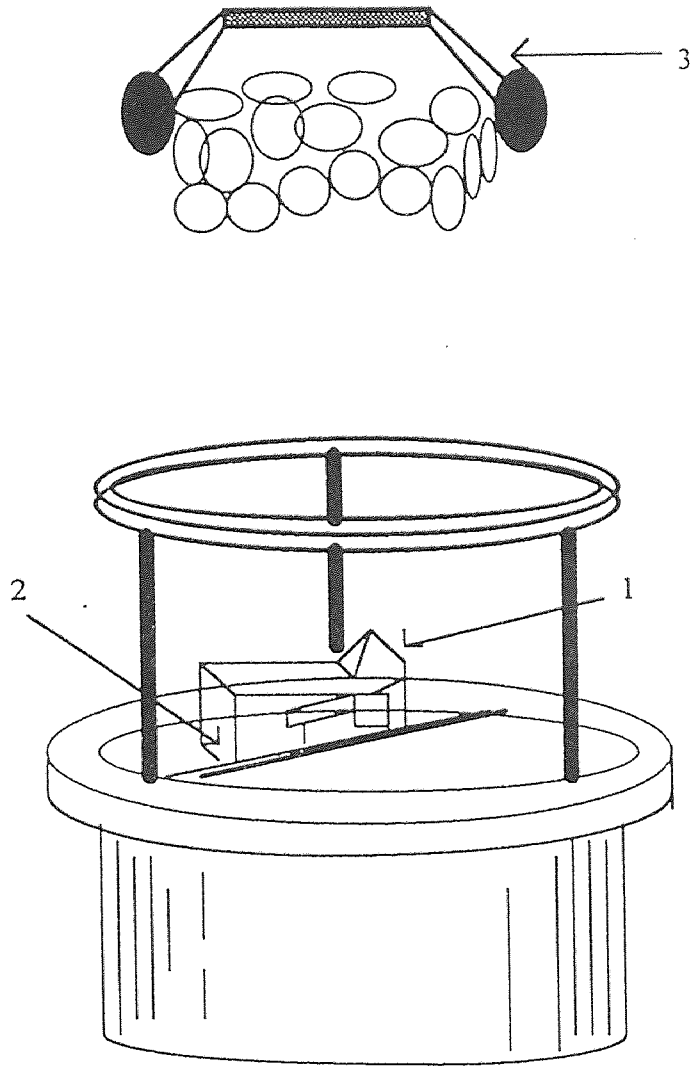


**Figure 3.2** Typical arrangement of electron-beam evaporator 1. of 270°C electron gun 2.centrally relatively to the planetary substrate holder 3.

### 3.2.3 Chemical Vapor Deposition (CVD)

In this technique, the material which forms a thin film on the substrate is produced by the chemical reaction that occurs on the substrate. The reaction is generally induced by heat, which causes either a decomposition of vapor or a reaction between different gaseous species in the ambient. Such decompositions are limited only by the availability of the reactants that are in the gas phase or that will easily vaporize. The reactants must decompose or react at temperatures that are low enough so that they do not effect the characteristics of the processed substrates.

Tungsten and molybdenum which are common metals for forming the silicides have been very successfully deposited using LPCVD (low-pressure chemical vapor deposition). The CVD for $WSi_2$ is generally performed in either a hot-wall low pressure system or a cold-wall low pressure system such as shown in Figure 3.3.

### 3.2.4 Sputtering

In the technique of sputtering using one composite target, the sputtering chamber has a single sputtering target. The Si:M ratio in the film is tied to that of the target and only small variations can be effected by changing the sputtering parameters. Figrue 3.4 shows the Si:Ta ratio of the Ta-Si films deposited using various sputtering pressures for the same sputtering target [29]. Thus, to obtain significant Si:M ratio variations, one must have several targets with Si:M ratios spanning the desired range.

In the technique of sputtering using two or more targets, the sputtering chamber can have two or more independently powered sputtering targets. In this case, the deposition rate is established from the individual metal and silicon targets for a given condition of sputtering. These rates are used to obtain the desired Si:M atomic ratio in the deposited silicide film.

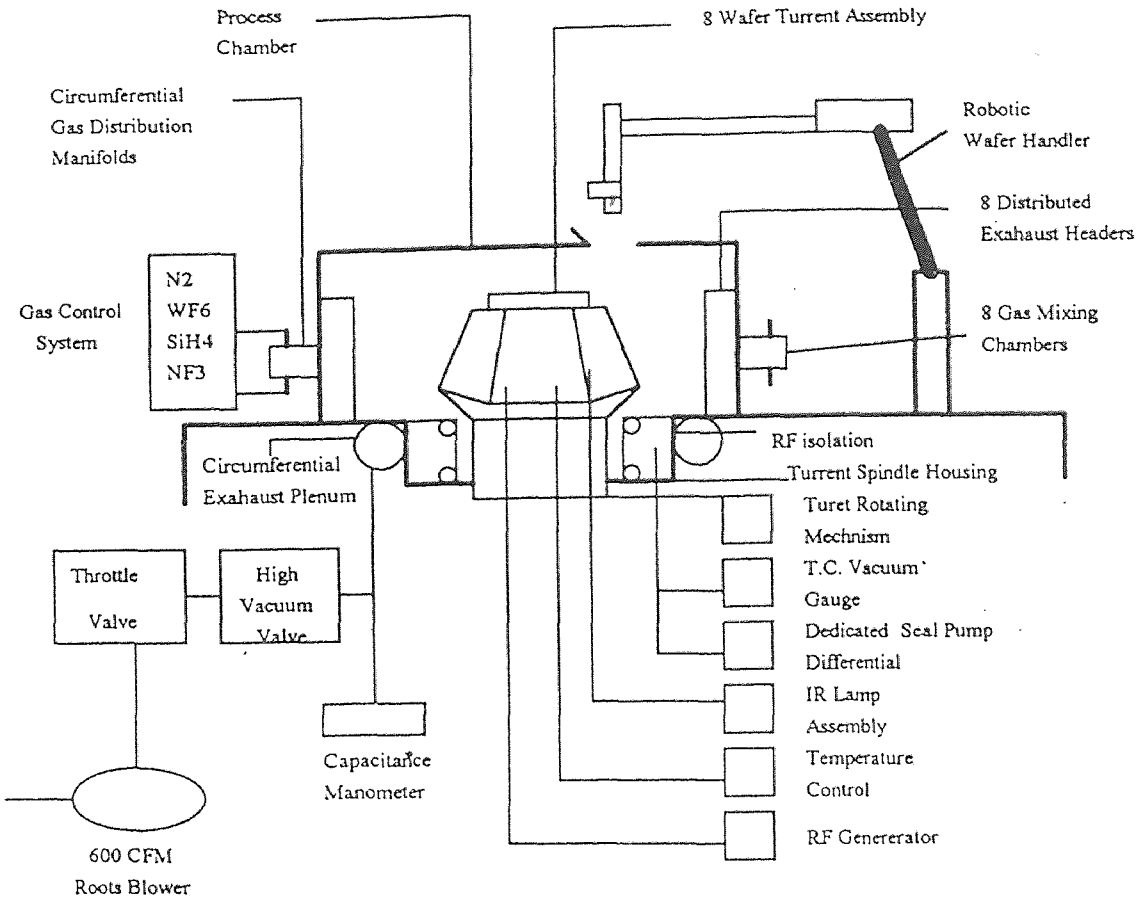


**Figure 3.3** Schematic of the cold-wall reactor for CVD of $WSi_2$

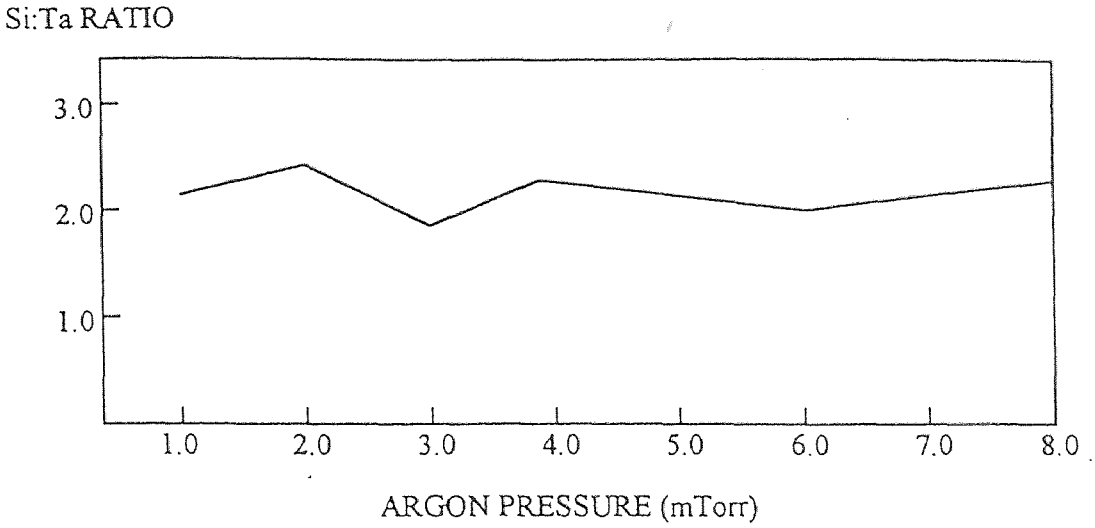


**Figure 3.4** Si:Ta ratio as a function of sputtering pressure on films obtained with target Si:Ta ratio of 2.6

### 3.2.5 Advantages and Disadvantages of Each of the Techniques

The technique of direct metallurgical reaction discussed in section 3.2.1 has one main advantage. The silicide growth from this method usually have a lower resistivity when compared to the other methods. Both polycide and silicide structures can be formed using this technique and the selective etching is possible. The disadvantage of this technique is that M/Si ratio which depends on the phase formed can not be easily controlled. The silicide formed from this technique is sensitive to sintering enviroment and after sintering, the surface formed can be rough.

The co-evaporation method have the following advantages. The purity of the silicide formed is relatively good and the sintering enviroment is not critical when compared to the other techniques. Moreover, the surface formed after sintering is quite smooth. However, the control of M/Si ratio is very difficult and step coverage is poor.

CVD method offers several advantages, the most important of which are exellent step coverage and high thoughput, higher purity films (low $O_2$ content), and improved uniformity on large area silicon wafers. Possible poor adhesion is the disadvantage.

Sputtering has these advantages : improved step coverage, good sintering enviroment, good step coverage, and trustworthy control of M/Si ratio. Among the various sputtering techniques, the sputtering from a composite target is a promising technology and has been extensively used for deposition of molybdenum silicide and tungsten silicide and polycide gates in VLSI because high quality films can be deposited with high throughput. The disadvantages are the contamination from a target.

## 3.3 Properties of Tantalum Silicide

The recent interests in micro electromechanical systems necessitated a closer look at the transition-metal silicides, including to their thermodynamics, electrical and mechanical properties, and their stability at very high temperatures. Among the transition-metal silicides, tantalum silicide has very attractive electrical and micromechanical characteristics. It is a low resistance material compared with polysilicon (approximately an order of magnitude lower). It has a very high electromigration activation energy which is 1.7 eV [3] (this is almost three times higher than aluminum of which electromigration activation energy is about 0.6 eV), which this eliminates the reliability problem caused by electromigration. It is comparable with standard IC processing techniques, and the hardness of $TaSi_2$ is significantly higher than that of many other silicides. Listed below are some of the characteristics of the tantalum silicide which make it favorable for the micro sensors and actuators applications:

(1) $TaSi_2$ has become a standard material in MOS processing technology [30]
(2) Good adhesion to silicon, silicon nitride and oxide
(3) Low resistivity : 35 - 55 $\mu\Omega$-cm
(4) No reaction with aluminum up to 500°C
(5) As hard as steel : hardness = 1402 kg/mm$^2$ (Table 3.2)
(6) Thermally stable : TCE = 8.8 ppm/°C (Table 3.2)
(7) Insoluble in $H_2SO_4 + H_2O_2$ mixture
(8) Good etch resistance in HF, primary wet etchant of $SiO_2$ (i.e. sacrificial layer)
(9) Very high electromigration activation energy : 1.7 eV
(10) Hard to form a native oxide layer [31]

Table 3.2 also shows that melting points of tantalum silicide is higher than any other silicides. Table 3.3 reveals the crystal structure of the tantalum silicide family [32].

**Table 3.2** Basic constants of silicides and elements

| Material | Thermal expansion coefficient (ppm/°C) | Mirohardness ($kg/mm^2$) | Melting point (°C) |
|---|---|---|---|
| Si | 3 | 850 | 1420 |
| Ti | 8.5 | 775 | 1661±10 |
| Ta | 6.5 | 935 | 2997 |
| Mo | 5 | 890 | 2617 |
| W | 4.5 | 860 | 3411 |
| $TiSi_2$ | 12.5 | 892 | 1540 |
| $TaSi_2$ | 8.8-10.7 | 1402 | 2200±100 |
| $MoSi_2$ | 8.25 | 1200 | 1980 |
| $WSi_2$ | 6.25-7.9 | 1074 | 2165 |

**Table 3.3** Crystal structure of the tantalum silicide family

| Silicide | Structure | Lattice constant (Å) | Density (g/cm2) |
|---|---|---|---|
| $TaSi_2$ | Hexagonal | a= 4.7821, c=6.5695 | 9.08 |
| $Ta_2Si$ | Teragonal | a=6.175, c=5.039 | 13.544 |
| $Ta_5Si_3$ | Teragonal | a=9.88, c=5.06 | 13.401 |

# CHAPTER 4

# INVESTIGATION OF THE MICROSTRUCTURE OF MAGNETRON-SPUTTERED THIN FILM

## 4.1 Magnetron Sputtering

### 4.1.1 What is Sputtering

Sputtering has been widely used as a metallization technique in VLSI. Sputtering is a physical phenonmenon involving the acceleration of ions, usually $Ar^+$, through a potential gradient, and the bombardment by these ions of a "target" or cathode. Through momentum transfer, atoms near the surface of the target material become volatile and are transported as a vapor to the substrates. At the substrates, the film grows through deposition. Conventional sputtering has found wide application in IC processing. Metals such as Al, Ti, Pt, Au, Mo, W, Ni, and Co are readily sputtered using either a dc or rf discharge in a diode system. A high electron density is required in the discharge to increase the ion current density at the target surface and thus prevent the oxide from forming. The high density may be achieved by introducing an auxiliary discharge, as in triode sputtering, or through the use of magnetic fields to capture the electrons and increase their ionizing efficiency, as is done in magnetron sputtering.

Some characteristics of sputter deposition are: (1) the ability to deposit alloy films with composition similar to that of the target, (2) the incorporation of Ar(~2%) and background gas(~1%) in the film, and (3) in conventional diode systems, considerable heating of the substrates (~350°C) by the secondary electrons emitted by the target. Often rf energy may be applied to the substrates which cause them to be bombarded by ions. If the rf is applied prior to metal deposition, the process is termed "sputter etching". Sputter etching may clear residual films from

window areas and enhance the contact between the metal and substrate. If the negative bias is applied to substrate during film deposition, it is a bias-sputter deposition, and may enhance the step coverage of the film or reduce the severity of the surface topography.

### 4.1.2 Various Effects of Sputtering

When a solid surface is bombarded by energetic ions, numerous effects may occur: (1) emission of neutral(sputtered) particles; (2) emission of secondary electrons; (3) emission of positive and/or negative ions; (4) emission of electromagnetic radiation; (5) reflection of incident particles; (6) desorption of gases; (7) implantation of incident particles; (8) heating; (9) chemical dissociation; (10) bulk diffusion; (11) crystallographic changes; and (12) reflection of some emitted species back to the target surface either by collision in the gas discharge of electrostatic attraction. Since the target is held at high negative potential, secondary electrons are emitted at target potential and accelerated toward the substrate. Upon arrival, such energy as they retain after colliding with sputtering gas atoms is liberated at the substrate in the form of heat.

It is highly improbable that a positive target ion generated at the target surface could escape the negative field. Honig[33] has shown that the fraction of positive ions originating at the target surface that escape the target field is very small(<1%) and the escape mechanism is very complex. The number of positive ions that are produced and, hence, can escape, is larger for compounds than for monatomic targets. Benninghoven[34] has shown that this occurs because of dissociation reactions in which the primary bombardment breaks down molecules into positive and negative ions that are then sputtered. He showed that the number of positive and negative ions released from metal targets decreases to a negligible minimum as the surface oxides on the target are sputtered away. Negative ions

produced by dissociation reactions are repelled from the target and accelerated toward the substrate. The ions may be neutralized by stripping collisions in the gas.

We have noted above that numerous energetic particles(electrons, ions, and neutrals) are liberated from the target and propelled toward the substrates. If bombardment by these particles is undesirable, high gas pressure can aid in slowing these particles to minimize substrate heating and other effects. In some cases, it is desirable to maximize the bombardment, thus dictating the use of low gas pressure.

It was shown above that the likelihood of a positive target ion escaping the target field is very small. However, it is entirely possible to create positive target ions by collisions in the rf glow discharge. This is less a problem in dc- than rf-glow discharges because of the higher ionization probability in the latter.

The probability that ions so produced would be neutralized before arriving at the substrate is very small. Positive ions and electrons recombine more readily at solid surfaces than in the gas discharge because both momentum and energy can be conserved with greater ease in a three-body collision (ion, electron, and surface) than in a two-body collision (ion and electron). Hence ions of target material produced in this manner may bombard the substrate surface, or in some cases, return to the target to cause self-sputtering.

### 4.1.3 Properties of Magnetron Sputtering

A typical magnetron sputtering process shown in Figure 4.1 has a shaped and closed path magnetic field to trap and concentrate the electrons produced in the discharge at the target surface. The electrons are confined to the space near the target. The high density cloud of electrons promotes ionization of the sputtering gas in the region close to the target surface, and the target is negatively biased to attract ions to the target. The high energy impact of these ions on the target dislodges atoms from the material which are collected on the substrate surface. Due to the

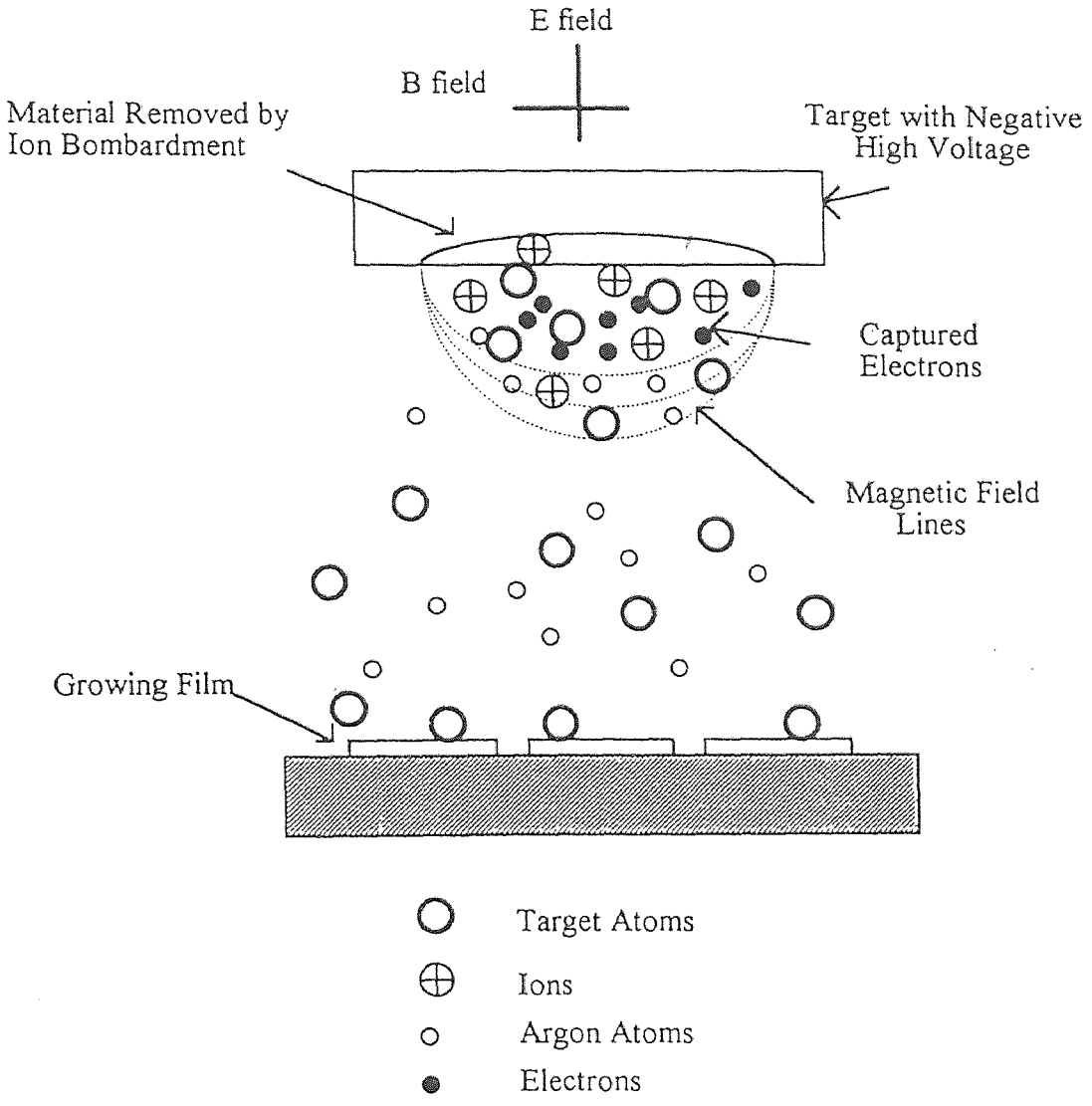


**Figure 4.1** Basic operation of magnetron sputtering system

high ionization efficiency of this process, low power levels may be used, and at the same time high deposition rates are achieved. Because electron leakage is restricted by the magnetic field, electron bombardment of the substrate is minimized and heating of the growing film and substrate is substantially reduced.

The magnetron sputtering process has many advantages [35,36]. The primary advantages are:

(1) high deposition rate,

(2) ease of sputtering any metal, alloy, or compound,

(3) high-purity of the deposited films,

(4) good adhesion of films,

(5) excellent coverage of steps and small features,

(6) ability to coat heat sensitive substrates,

(7) ease of automation, and,

(8) excellent uniformity on large area substrates.

Magnetron sputtering, because of the above advantages, is a very powerful technique which can be used in a wide range of applications.

## 4.2 Microstructure of Sputter-Deposited Films

### 4.2.1 Columnar Grain Structure

The columnar grain structure of thin films has been a subject of interest for several decades. This microstructure consisting of a network of low-density material surrounding an array of parallel rod shaped columns of higher density has been much studied by transmission and scanning electron microscopy. Columnar structures grow when the mobility of deposited atoms is limited. They have been observed in high-melting point materials (Cr, Be, Si, and Ge), in compounds of high binding energy (TiC, TiN, $CaF_2$, and PbS), and in non-noble metals evaporated in the presence of oxygen (Fe and Fe-Ni). Amorphous films of Si, Ge,

SiO, and rare earth-transition metal alloys (Gd-Co), whose very existence depends on limited adatom mobility, are frequently columnar when deposited at sufficiently low temperature. Magnetic, optical, electrical, mechanical, and surface properties of films are affected, sometimes strongly, by columnar structures.

### 4.2.2 Zone Models for Sputtered Films

An essential feature of thin films is that they are formed from a flux that approaches the substrate from a limited set of directions. Furthermore, at low homologous temperature $T$, relative to coating material melting point $Tm$ a growth structure defined by columnar voided boundaries is superimposed on the intrinsic grain structure as shown in Figure 4.2(a). Thus thin film microstructures tend to have an anisotropic character which influences such properties as their magnetic anisotropy and their effectiveness for lateral current transport and as diffusion barriers. For example, the grain or growth boundaries present preferred diffusion paths which often extend through the entire coating thickness. (Activation energies for surface, grain boundary, and bulk diffusion are typically in the ratio 1:2:4 so that at $T/Tm < 0.5$ surface and grain boundary diffusion rates can be orders of magnitude larger than bulk diffusion rates.)

It is useful to envision coating growth as proceeding in three general steps as indicated schematically in Figure 4.2(b). The first step involves the transport of the coating species to the substrate. The second step involves the adsorption of these species onto the surface of the substrate or growing coating, their diffusion over this surface, and finally their incorporation into the coating or their removal from the surface by evaporation or sputtering. The third step involves movement of the coating atoms to their final position within the coating by processes such as bulk diffusion. In the case of sputter deposition, the transport step is controlled by parameters such as the apparatus geometry and working gas pressure, while the

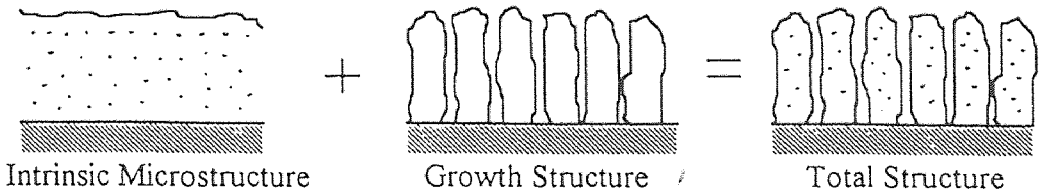


(a)

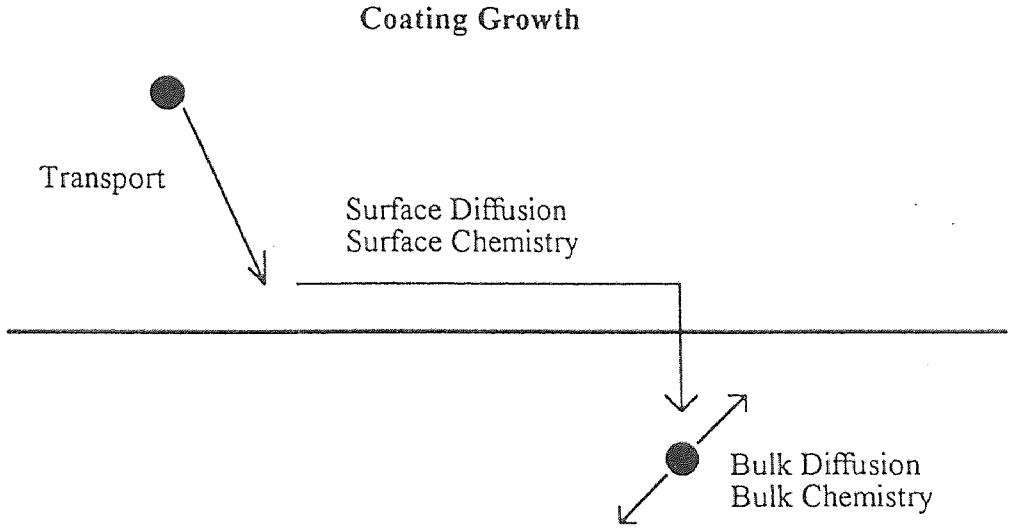


(b)

**Figure 4.2** Schematic illustrations showing (a) the superposition of growth and microstructures for films deposited under conditions of low adatom mobility (b) the steps involved in the condensation of a vapor during film growth

diffusion steps are controlled largely by the substrate temperature, but may be significantly influenced by energetic particle bombardment.

Structure-zone models have proven very useful in providing an overview of the relationship between the microstructure of vacuum deposited coatings and the most prominent deposition parameters. The first such model was published by Movchan and Demchisshin (MD) in 1969. MD found that the microstructures of thick(0.3 to 2mm) evaporated coatings of Ti, Ni, W, ZrO and $Al_2O_3$ could be represented as a function of *T/Tm* by three zones, each with its own characteristic structure and physical properties. The low temperature ($T/Tm < 0.3$) zone1 structure was columnar, consisting of tapered units defined by voided growth boundaries of the type shown in Figure 4.2(a). The zone 2 structure ($0.3 < T < 0.5$) consisted of columnar grains, which were defined by metallurgical grain boundaries and increased in width with *T/Tm* in accordance with activation energies typical of surface diffusion. The high temperature zone 3 ($T/Tm > 0.5$)structure consisted of equiaxed grains, which increased in size in accordance with activation energies typical of bulk diffusion.

In 1973 the zone model was extended to magnetron sputtered metal films by adding an axis to account for the effect of the Ar working gas pressure as shown in Figure 4.3 [37,38]. The model was based on an examination of 0.025 to 0.25 mm thick coatings of Ti, Cr, Fe, Cu, Mo, and Al alloy deposited onto glass substrates using magnetron sputtering sources. In this model, the MD zones were associated with conditions where the physics of coating growth was dominated in turn by mechanisms associated with each of the three steps shown in Figure 4.2 (b)-zone 1, atomic shadowing during transport; zone 2, surface diffusion; and zone 3, bulk diffusion. A fourth zone consisting of a dense array of poorly defined fibrous grains was identified in the region between zone 1 and 2 and termed zone T since it was believed to be a transition state between the two MD zones.

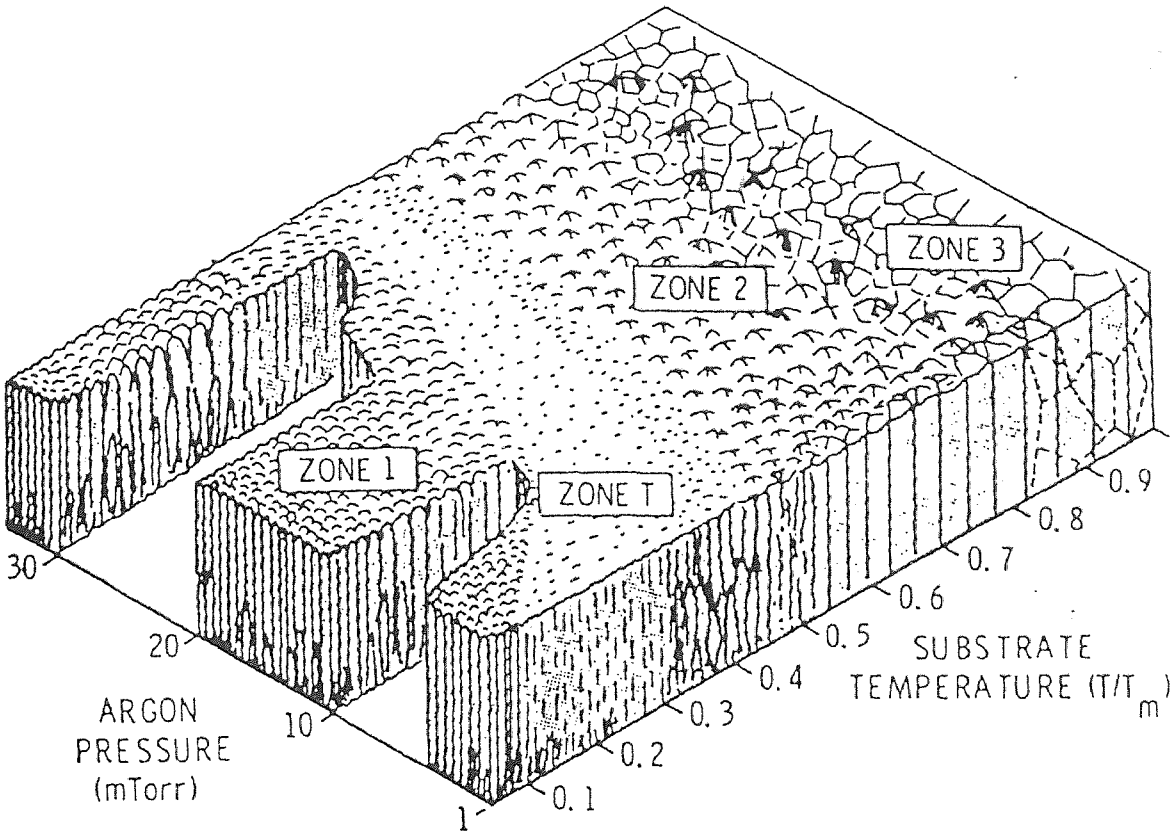


**Figure 4.3** Microstructure zone diagram for metal films deposited by magnetron sputtering. T is the substrate temperature and Tm is the coating material melting point.

### 4.3 Stresses in Magnetron-Sputtered Thin Films

The results of extensive studies by Hoffman and Thornton [39,40,41] on magnetron-sputtered metal films are particularly instructive since the internal stress correlates directly with microstructural features and physical properties. Magnetron sputtering sources have made it possible to deposit films over a wide range of pressures and deposition rates in the absence of plasma bombardment and substrate heating. It was found that two distinct regimes, separated by a relatively sharp boundary, exist where the change in film properties almost discontinuous (Figure 4.4 and 4.5). The transition boundary can be thought of as a multidimensional space of the material and processing variables involved. On one side of the boundary, the films contain compressive residual stresses and entrapped gases, but exhibit near-bulklike values of electrical resistivity and optical reflectance. This side of the boundary occurs at low sputtering pressures, with high mass targets, and low deposition rates. On the other hand, elevated sputtering pressures, light target metals, and oblique incident angle of the depositing flux favor the generation of films possessing tensile stresses containing lesser amounts of entrapped gases.

Comparison with the microstructure of sputtered films reveals that elevated working pressures are conducive to development of columnar grains with intercrystalline voids. Such a structure exhibits high resistivity, low optical reflectivity, and tensile stresses. At lower pressures the development of the columnar structure with voids is suppressed. Energetic particle bombardment, mainly by sputtered atoms, apparently induces compressive film stress by an atomic peening mechanism.

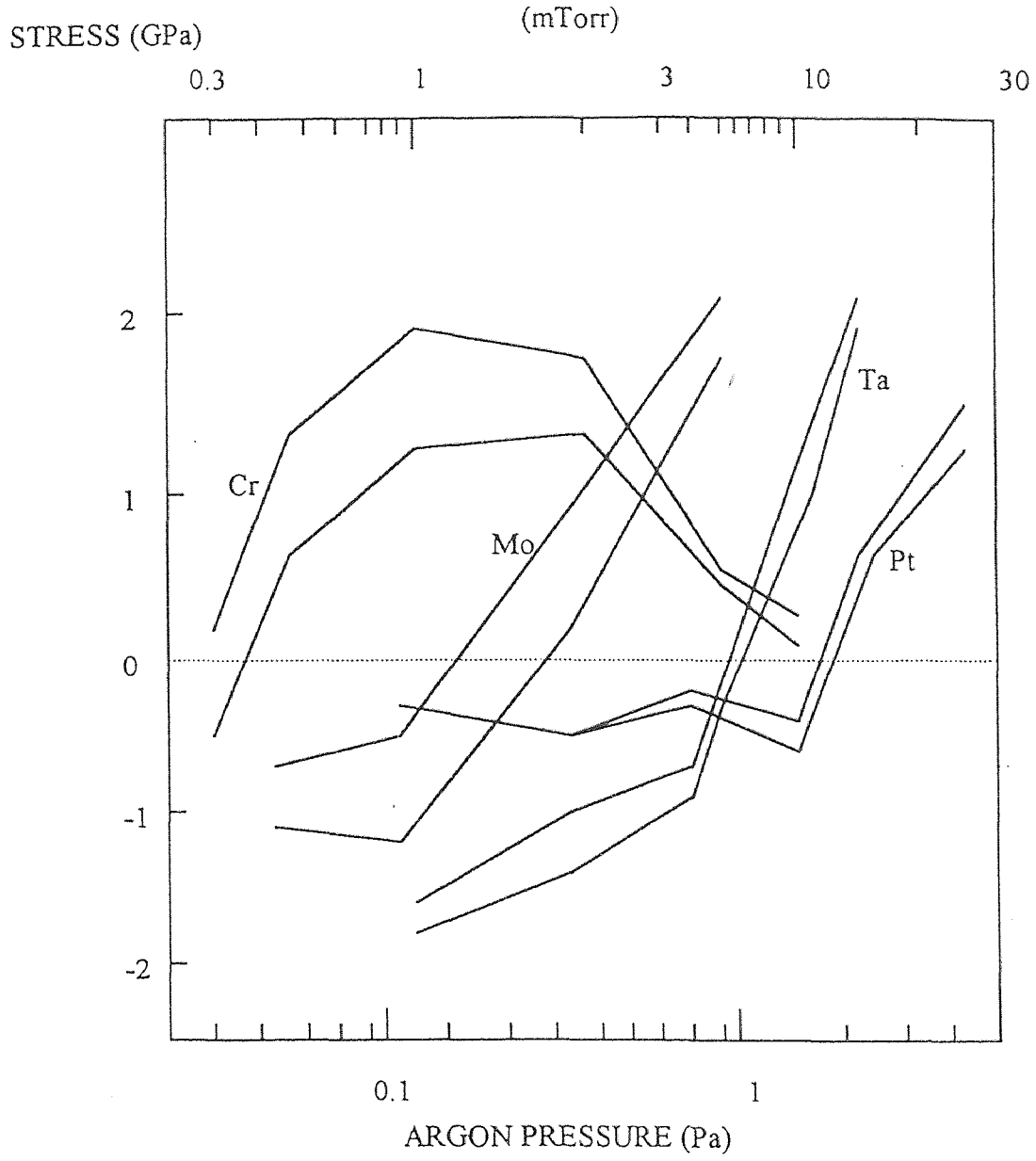


**Figure 4.4** Biaxial residual stresses as a function of Ar pressure for Cr,Mo,Ta, and Pt films sputtered onto silicon substrate

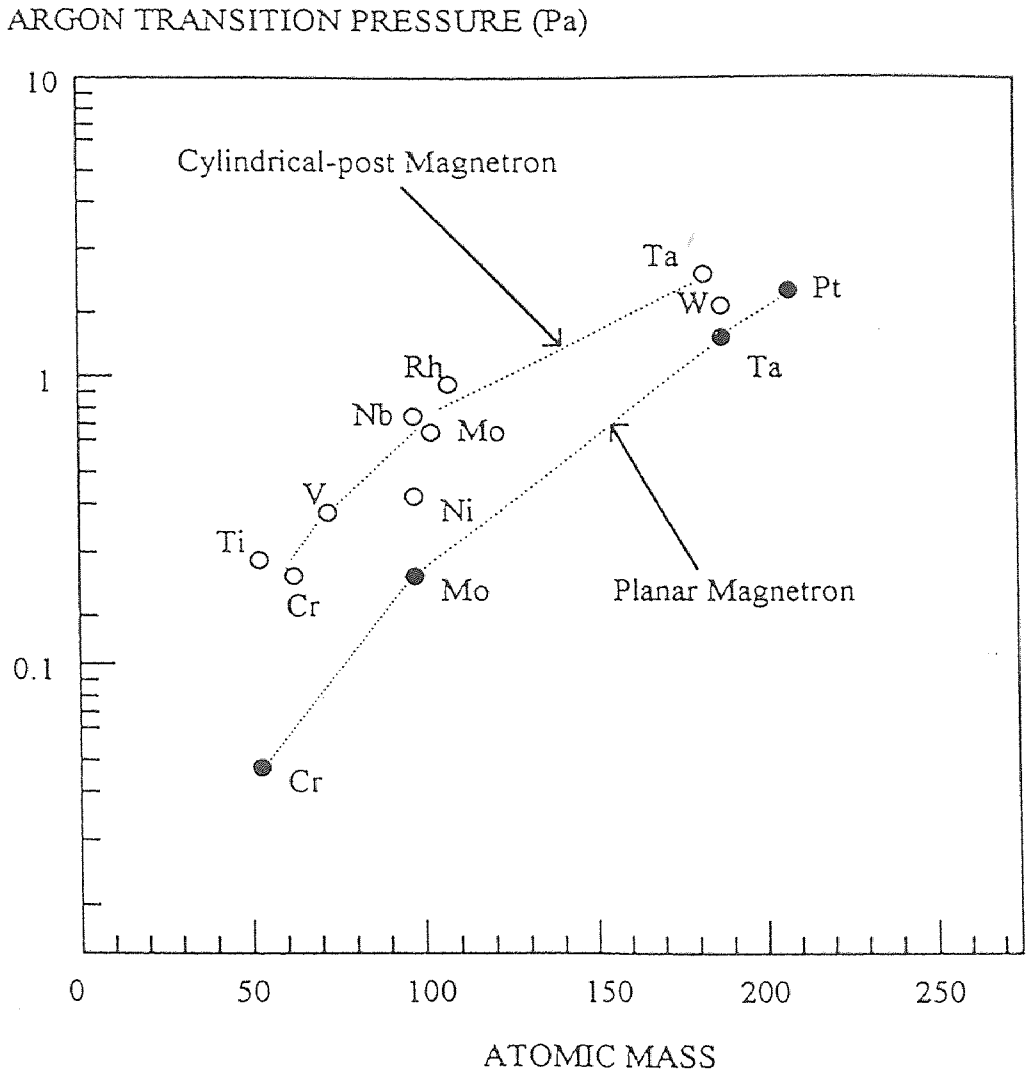


**Figure 4.5** Argon transition pressure vs atomic mass of sputtered metals for tensile to compressive stress reversal

# CHAPTER 5

# EXPERIMENT

## 5.1 Wafer Cleaning and Sputter Deposition

Four silicon substrates were piranha cleaned ( P-clean, 5:1 $H_2SO_4$ : $H_2O_2$ ) for 10 minutes at 110°C to remove any organic residues on the wafers. Then the wafers were rinsed in hot deionized (DI) water for 10 minutes followed by cold DI water rinse for 5 minutes. In addition, the silicon wafers were dipped into a 100:1 $H_2O$:HF mixture immediately before they were loaded into the sputtering chamber to etch off the native oxide after the acid cleaning.

A magnetron-type dc sputtering source with a composite target (Varian 3125 magnetron sputtering system) was used to deposit tantalum silicide thin films. The sputter chamber was pumped to a vacuum of less than $8 \times 10^{-7}$ Torr before being back filled with argon gas. Four different deposition pressure ( 0.5, 3, 10, and 15 mTorr ) were selected to see the stress transition because the stress transition was expected to occur in this range [40]. Tantalum silicide thin films were deposited on 4-inch diameter silicon wafers, 525μm thick. The thickness of the silicide film was measured by a surface profilometer. The films deposited had approximately same thickness (0.5±0.05μm). The deposition temperature was measured by a thermocouple and its probe was placed within one inch above the substrate for an accurate measurement of the substrate surface temperature(In a conventional sputtering system, a temperature sensor is normally attached to the substrate holder.). Deposition parameters are given in Table 5.1.

**Table 5.1** Deposition parameters for tantalum silicide

| Parameter | Value |
|---|---|
| Steady State Substrate Temperature | 300°C |
| Base Pressure | $8.0 \times 10^{-7}$ Torr |
| Deposition Pressures | 0.5, 3, 10 and15 mTorr |
| Backfill Gas | Argon |
| Deposition Rate | 2-4 Å/second |
| Target Composition | $TaSi_{2.4}$ |

## 5.2 Measurements

Stress in the tantalum silicide films was calculated from wafer curvature measured by laser beam method shown in Figure 5.1. Two circular spots were produced from the two laser beams and were projected on substrate/film by a mirror, then the reflection from the surface of the wafer was projected again on the screen with scale by the mirror. The distance of the two spots on the screen reflected from the mirror was recorded before and after deposition. Finally, the average stresses of films were determined by the Stoney's formula.

Film resistivity were measured by the four-point probe technique. A very convenient way to measure the resistivity of a film is to lightly press a four-point metal-tip probe assembly into the surface as shown in Figure 5.2. The outer probes are connected to the current source, and the inner probes detect the voltage drop. Electrostatic analysis of the electric potential and field distributions within the film yields $\rho = KVI^{-1}d$, where d is a film thickness and K is a constant dependent on the configuration and spacing of the contacts. In my experiment, $K = \pi/\ln 2 = 4.53$ was chosen because the film is large in extent(100mm) compared with the probe assembly and the probe spacing(2.5mm) is large compared with film thickness (0.5μm) [41]. Table 5.2 shows the measured parameters.

**Table 5.2** Measured Parameters

| $P_{Ar}$(mTorr) | Δbefore | Δafter | $\sigma_a$(MPa) | I(mA) | V(mV) | ρ (μΩ-cm) |
|---|---|---|---|---|---|---|
| 0.5 | 106 | 135 | -713.4 | 0.833 | 0.30 | 81.6 |
| | | | | 1.666 | 0.71 | 96.5 |
| | | | | 2.500 | 1.13 | 102.4 |
| | | | | 3.332 | 1.56 | 106.0 |
| | | | | 4.165 | 1.57 | 85.4 |
| | | | | 5.000 | 1.69 | 76.6 |
| 3 | 123 | 130 | -172.2 | 0.833 | 0.33 | 89.7 |
| | | | | 1.666 | 0.90 | 122.3 |
| | | | | 2.500 | 0.96 | 87.0 |
| | | | | 3.332 | 1.65 | 112.2 |
| | | | | 4.165 | 2.02 | 109.9 |
| | | | | 5.000 | 2.31 | 104.6 |
| 10 | 113 | 91 | +541.0 | 0.833 | 0.67 | 182.2 |
| | | | | 1.666 | 1.46 | 198.5 |
| | | | | 2.500 | 1.59 | 144.0 |
| | | | | 3.332 | 2.43 | 165.2 |
| | | | | 4.165 | 2.72 | 149.1 |
| | | | | 5.000 | 3.62 | 164.0 |
| 15 | 119 | 103 | +393.6 | 0.833 | 2.72 | 310.0 |
| | | | | 1.666 | 3.33 | 317.7 |
| | | | | 2.500 | 3.54 | 320.7 |
| | | | | 3.332 | 4.01 | 272.6 |
| | | | | 4.165 | 6.53 | 355.1 |
| | | | | 5.000 | 6.97 | 315.7 |

* where, - and + denote compressive and tensile stress, respectively.

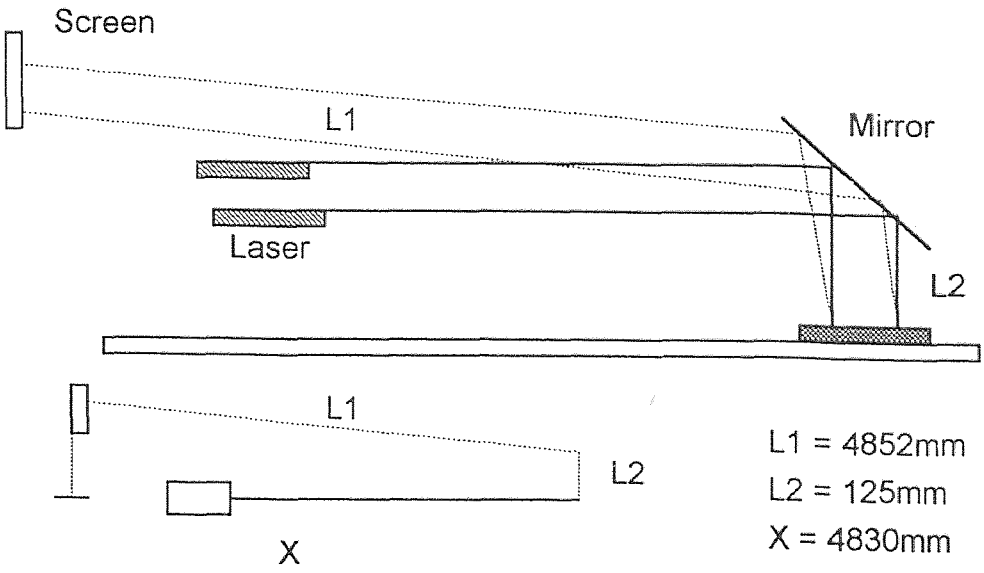


$$\text{stress}(\rho) = 12.3 \times (\Delta_{\text{before}} - \Delta_{\text{after}}) / tf$$

**Figure 5.1** Optical system for stress measurement in NJIT's Thin Film Characterization Laboratory

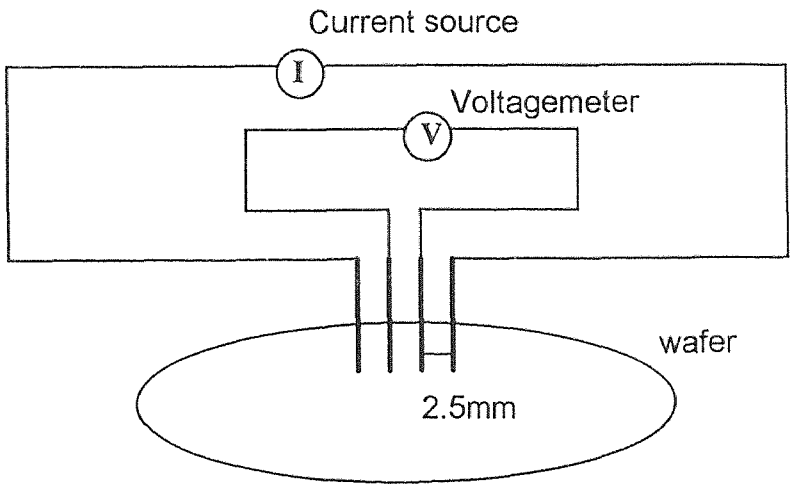


**Figure 5.2** Four-point probe method for resistivity measurement for thin films in NJIT's Optical Imaging Laboratory

# CHAPTER 6

# DISCUSSION

The deposited tantalum silicide thin films might have thermal stresses because films prepared at elevated temperatures and then cooled to room temperature would be thermally stressed. Assuming a biaxial stress state, the thermal residual stress contribution to the total measured stress can be established as $\sigma_f = \Delta\alpha\Delta T[E_f/(1-\nu_f)]$ [42], where $\Delta\alpha$ is the difference in the thermal expansion coefficients between film and substrate, $\Delta T$ is the temperature change after deposition (The steady state temperatures of substrates and films were assumed to be 300°C although the film temperature was expected to be slightly higher.) and $[E_f/(1-\nu_f)]$ is the biaxial elastic modulus of the $TaSi_2$ film. For $\Delta\alpha=5.8\times10^{-6}$°C, $E_f$=158GPa, and $\nu_f$=0.213 [43], the estimated thermal stress in these films is 320MPa. This value is less than the maximum residual tensile stress(541MPa) measured at 10mTorr. Therefore, the residual stress behavior of the films seemed to be dominated by an intrinsic stress arising from the incomplete structural ordering during film growth. Consequently, the stress analysis will be focused on the intrinsic stress behavior.

The intrinsic stress of the sputtered tantalum silicide thin films could be changed from highly compressive to highly tensile by varing the argon pressure. Figure 6.1 shows the thermal, intrinsic and measured residual stress of the films as a function of the argon pressure. It could be seen that the intrinsic stress was quite sensitive to the argon pressure. The intrinsic stress of the film deposited at the lowest working gas pressure (0.5mTorr) revealed maximum compressive (1033.4MPa). The transition pressure at which the intrinsic stress changes from compression to tension was about 8 mTorr. The maximum value for the tensile intrinsic stress(221MPa) was measured at 10mTorr. With further increase, the

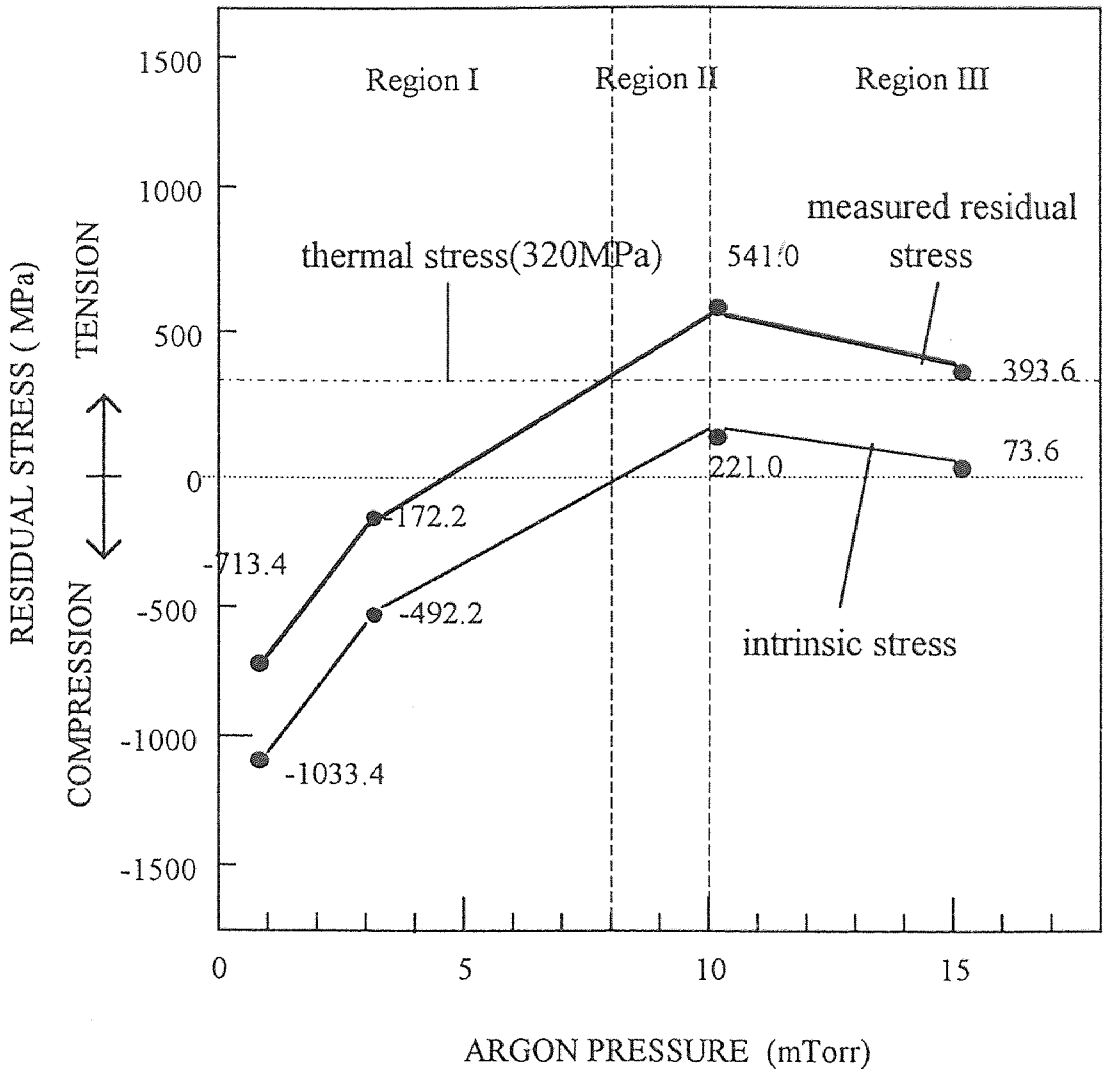


**Figure 6.1** Average residual stresses of tantalum silicide thin films at various $P_{Ar}$

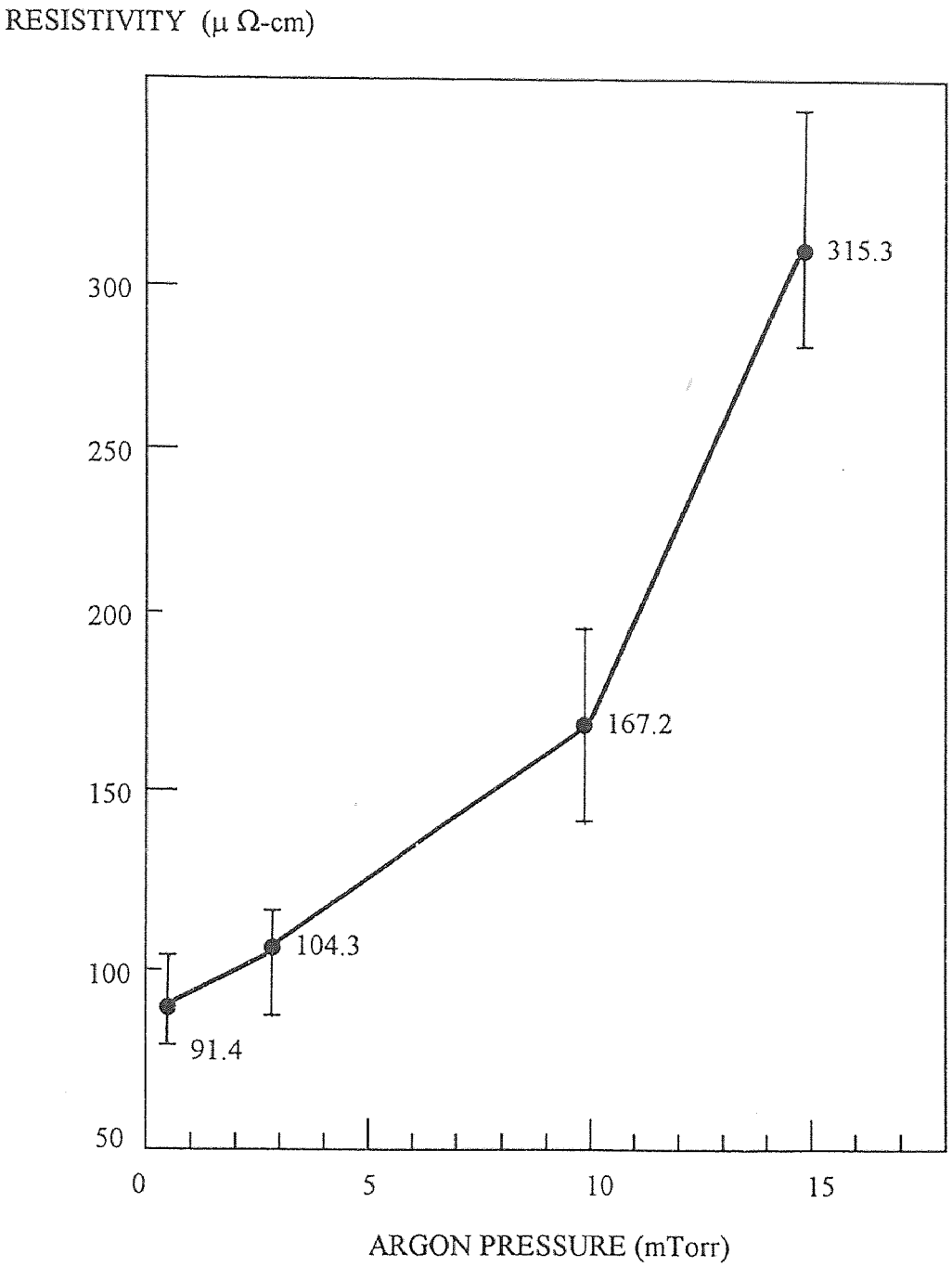


**Figure 6.2** Room temperature resistivity at various Ar pressure

**Figure 6.3(a)** Plan-view SEM micrograph of tantalum silicide thin film at 0.5mTorr

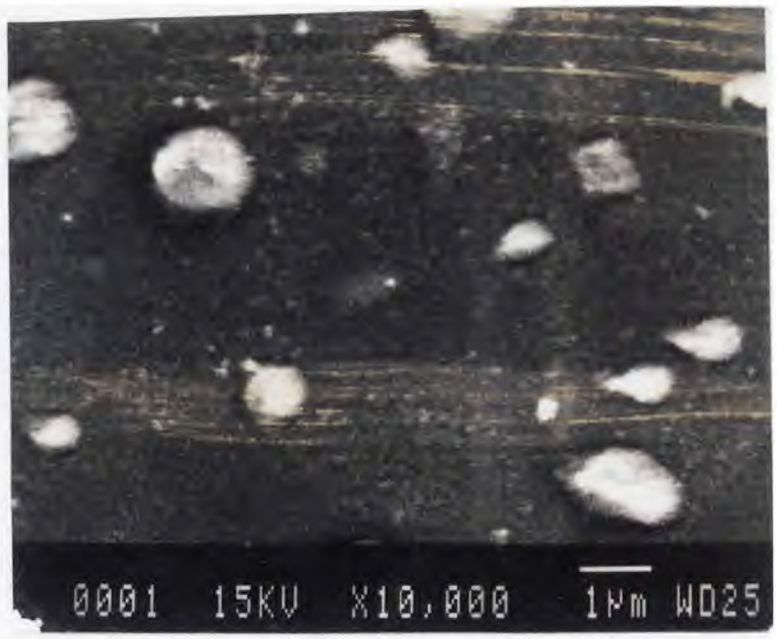


**Figure 6.3(b)** Plan-view SEM micrograph of tantalum silicide thin film at 3mTorr

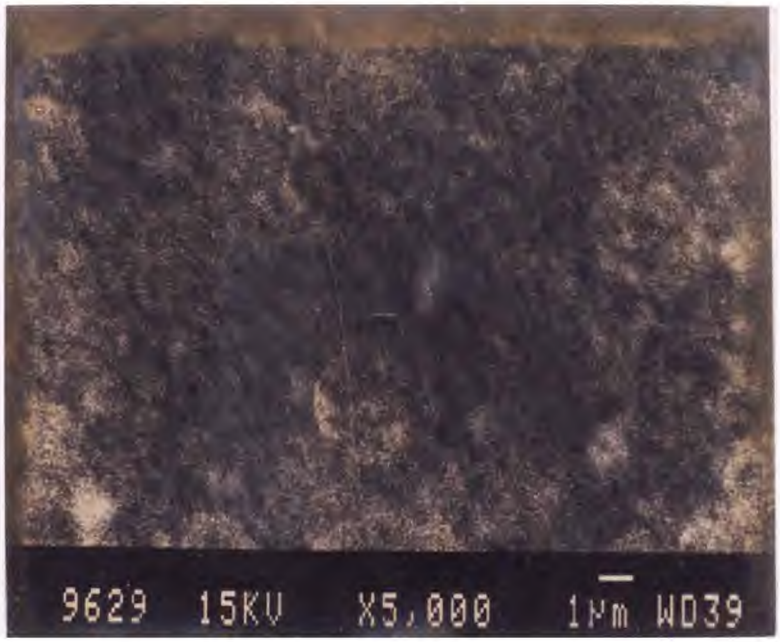


**Figure 6.3(c)** Plan-view SEM micrograph of tantalum silicide thin film at 10mTorr

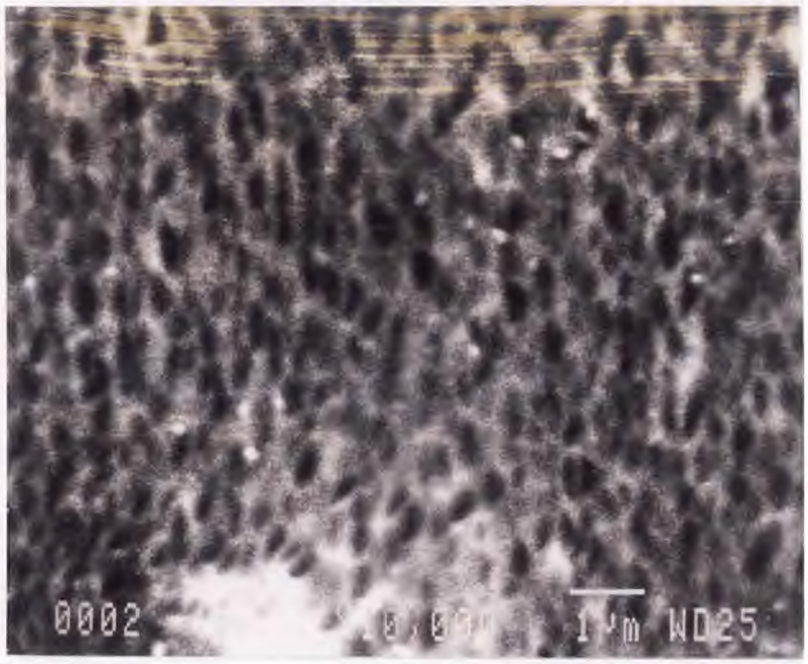


**Figure 6.3(d)** Plan-view SEM micrograph of tantalum silicide thin film at 15mTorr

tensile intrinsic stress of the film decreased to a value of 73.6MPa at 15mTorr. In the calculation of the stresses, Young's modulus Es of 130 GPa and a Poisson ratio $\nu_s$ of 0.280 were used [44]. For convenience, the range of argon pressure in Figure 6.1 was divided into three regions, namely Region I (0.5 ~ 8mTorr), Region II (8 ~ 10mTorr) and Region III (10 ~15mTorr).

At lower pressures (Region I in Figure 6.1), compressive intrinsic stresses (-713.4 and -172.2MPa) were observed. The cause of the compressive stress has been studied well by Thornton [45,46,47]. Since higher particle energies are expected for lower sputtering pressures due to the fewer collisions (i.e., larger mean free path), the energetic particle bombardment of the film during deposition may be the major factor for a compressive stress [42,45]. The energetic particles may be sputtered atoms or working gas atoms which are neutralized and reflected at the cathode or a combination of both [48,49,50]. There may be several ways in which the energetic particle bombardment can promote the compressive stress in the films.

Energetic particle bombardment, mainly by sputtered atoms, apparently induces compressive film stress by the bombardment of the film resulting in the film compression. The compressive stress is also caused by the lattice expansion induced by the incorporated energetic working gas particles into films. In fact, when the energetic ions, which are accelerated through a potential gradient, bombard the target, some incident ions are reflected and neutralized at the target surface (If not neutralized at the target, it is highly improbable that the reflected positive ions at the surface could escape the negative potential) and carried to the substrate. The energy flux carried to the substrate by neutralized and reflected ions depends on the cathode shape (because of the scattering directions of the reflected species)and the working gas pressure. The SEMs show that the surface of the film

deposited at 0.5mTorr is very smooth (Figure 6.3(a)), but some defects are observed in the film at 3mTorr (Figure 6.3(b)).

At intermediate pressures (Region II in Figure 6.1), tensile intrinsic stresses(0 ~ 221MPa) were found. Furthermore, as the argon pressure increased, the stress also increased. Figure 6.3(c) shows the plan-view SEM micrograph of the film deposited at 10mTorr. The surface of the film deposited at 10mTorr was similar to that of the film deposited at 3mTorr, that is, the surface was not smooth and grains were not observed. Therefore, we could think that the argon pressure was still low enough to compress the growth structure through the energetic particle bombardment effects. Of course, we could also think that the mobility of sputtered atoms was high enough to fill in the gaps between grains, or the self-shadowing at grain edges was negligible.

At higher argon pressures (Region III in Figure 6.1), it was observed that as $P_{Ar}$ increased, the tensile intrinsic stress decreased to 73.6MPa. This phenomenon can be explained by the relaxation of the interforces acting between grains[51]. The presence of less dense regions during film growth may result in a tensile film stress due to the interforces which pull together. However, as the distance between the grains increases, the grains are no longer pull together and bring the relaxation of the tensile intrinsic stress. The SEM of the film at 15mTorr showed relatively large gaps between grains. However, although some gaps and grains were observed in this growth structure, the structure was an equiaxed structure rather than a complete columnar structure, that is, the diameter of grains was comparable to the thickness of the film. Therefore, we can think that the more columnar structure (i.e. more gaps) may be grown at higher argon pressure (because of the less energetic particle bombardment , or the more shadowing effect) or at lower temperature (because of the lower mobility of sputtered atoms).

Figure 6.2 shows the electrical resistivity of the films sputtered at various pressures. From the graph, we can see that as the argon pressure increases, the resistivity increases faster. The change of resistivity with respect to argon pressure seemed to be closely related to the growth structure of films. Thus, the sudden change of the increasing rate may be explained by the sudden change of growth structure. Unlike the intrinsic stress behavior, resistivity increased continuously although the slope changed suddenly into a higher value. Therefore, it may be concluded that the resistivity is affected by the microstructure of the film.

# CHAPTER 7

## CONCLUSION

(1) The stress versus argon pressure reveals the stress transition from compression to tension and tensile stress maximum.

(2) Tantalum silicide thin film can be prepared in any stress state (tensile, stress-free or compressive) by varying the argon pressure, i.e., the residual stress of tantalum silicide film is sensitive to the argon pressure.

(3) The cause of compressive residual stress can be explained by energetic particle bombardment at low gas pressures, i.e., the bombardment of films and the incorporation of working gas into films.

(4) At the highest pressure, the appearance of relatively large gaps between grains may dominate the stress behavior and cause the relaxation of tensile residual stress.

(5) The resistivity of the tantalum silicide thin film reveals a sputtering-pressure dependence and seems to be closely related to the microstructure of films.

## REFERENCES


[1] W. D. Nix, "Mechanical Properties of Thin Film," *Met. Trans.*, vol. 20A, p. 2217, 1989.

[2] D. W. Hoffman, "Perspective on Stresses in Magnetron-sputtered Thin Films," *J. Vac. Sci. Tech.*, A12(4), pp. 953-961, Jul/Aug 1994.

[3] S. P. Murarka, *Silicide for VLSI Application*, Academic Press, New York, NY, 1983.

[4] R. P.Vinci and J. C. Bravman, "Mechanical Testing of Thin Films," *Tranceducers*, p. 943, June 91.

[5] G. G. Stoney, "Stress in Thin Film," *Proc. Roy. Soc.*, A82, p. 172, 1909.

[6] D. S. Campbell, "Mechnical Properties of Thin Films," *Handbook of Thin Films*, McGraw Hill, New York, NY, 1970.

[7] K. Kinosita, *Proc. 2nd Coll. on Thin Films*, Vandenhoeck and Ruprecht, Gottinggen, p. 31, 1968.

[8] M. Laugier, "The Construction and Use of Thin Film Thermocouples for the Measurement of Surface Temperature Determination and Themal Bending of Cantilevered Plate During Film Deposition," *Thin Solid Films*, vol. 67, p. 163, 1980.

[9] J. A. Thornton and A. S. Penfold, *Thin Film Process*, Academic Press, New York, NY, 1978.

[10] P. A. Flinn, "Principles and Applications of Wafer Curvature Techniques for Stress Measurement in Thin Films, *Mat. Res. Soc. Symp. Proc.*, vol. 130, p. 41, 1989.

[11] C. S. Barrett and T. B. Massalski, *Structure of Metals*, McGraw-Hill, New York, NY, p. 234, 1966.

[12] H. P. Klug and L. H. Alexander, *X-Ray Diffraction Procedures*, Wiley, New York, NY, p. 143, 1974.

[13] A. Taylor., *X-Ray Metallography*, Wiley, New York, NY, 1961.

## REFERENCES
**(continued)**

[14] J. T. Norton, "Norelco Reporter," *IEEE Trans. Electron Device*, p. 50, April-June 1968.

[15] J. T. Norton, "Material Evaluation," *IEEE Trans. Electron Device*, p. 9, February 1973.

[16] M. E. Hilley and R. E. Rickefs, "Residual Stress Measurement by X-ray Diffraction," *SAE information Report*, p. 784, 1971.

[17] H. Kotake and Shin Takasu, "Quantitive measurement of stress in silicon by photoelasticity and its application," *J. Electrochem. Soc.*, vol. 127, p. 179, January 1980.

[18] S. P. Murarka, *Silicide for VLSI Application*, Academic Press, New York, NY, 1983.

[19] R. Wehnmann, *High-temperature Materials and Technology*, Wiley, New York, NY, 1967.

[20] D. Pramanik and A. N. Saxena, "VLSI Metallization using Aluminum and its Alloys," *Solid State Technology*, No.1, p. 127, 1983.

[21] S. M. Sze, *VLSI Technology*, Wiley, New York, NY, pp. 372- 376, 1988.

[22] J. M. Andrews, "Electrical Conduction in Implanted Polycrystal silicon," *J. Electron Materials* , No. 3, p. 227, 1980.

[23] D. M. Brown, W. E. Engler, M. Garfinkel and P. V. Gray, "Metallization in VLSI," *Solid State Electronics*, vol. 11, p. 1105, 1986.

[24] W. Moffat, *Handbook of Binary Phase Diagrams*, General Electric Co., New York, NY, 1978.

[25] S. P. Murarka, "Refractory Silicides for Integrated Circuits," *J. Vacuum Science and Technology*, vol. 17, p. 775, 1980.

[26] S. P. Murarka, "Formation of Silicides," *IEEE in IEDM Technology*, p. 454, 1979.

## REFERENCES
## (continued)

[27] S. P. Murarka, *Silicide for VLSI Application*, Academic Press, New York, NY, p. 151, 1983.

[28] S. Wolf and R. N. Tauber, *Silicon Processing for VLSI Era*, Lattice Press, Torance, CA, 1990.

[29] S. Inove and N. Ishika, "Effect of Si:Ta Ratio on Sputter Deposition of Silicides," *J. Electrochem. Soc.*, vol. 128, p. 2402, 1981.

[30] A. C. Adams, "Dielectric and Polysilicon Film Deposition," *VLSI Technology*, McGraw Hill, New York, NY, p. 93, 1983.

[31] S. P. Murarka, *Silicide for VLSI Application*, Academic Press, New York, NY, p.135, 1983.

[32] S. P. Murarka, *Silicide for VLSI Application*, Academic Press, New York, NY, p. 137, 1983.

[33] R. Honig, "Properties of Magnetron Sputtering," *J. Appl. Phys.*, vol. 29, p. 549, 1985.

[34] A. Benninghoven, "Dissociation Reactions in Sputtering," *Z. Physik*, 220, p. 159, 1969.

[35] D. W. Hoffman, "Perspective on Stresses in Magnetron-Sputtered Thin Films," *J. Vac. Sci. Technol.*, A12(4), pp. 953-962, 1994.

[36] J. A. Thornton, "The Influence of Bias Sputter Parameters on Copper Coating," *Thin Solid Films*, vol. 40, p. 335, 1977.

[37] J .A. Thornton, "Residual Stresses in Sputtered Ti Films," *J. Vac. Sci.*, vol. 12, p. 830, 1975.

[38] J. A. Thornton, "Mechanical Properties of Sputter Deposited Films," *Annu. Rev. Mater. Sci.*, vol. 7, p. 239, 1977.

[39] J. A. Thornton and D. W. Hoffman, "Residual Stress Analysis on Planar Sputtering Films," *Thin Solid Films*, vol. 171, p. 111, 1979.

## REFERENCES
## (continued)

[40] J. A. Thornton and D. W. Hoffman, "Stress Behavior in Metal Films," *J. Vac. Sci. Technol.*, vol. 18, p. 203,1977.

[41] J. A. Thornton and D. G. Cornog, "Indum Doped Cadium Sulfide Films," *J. Vac. Sci. Technol.*, vol. 18, p. 199, 1981.

[42] A. C. Westerheim, "In-situ Substrate Temperature Measurement in High Tc Super Superconducting Film Deposition," *J. Vac. Sci. Technol.*, vol. 11(6), p. 3020, 1993.

[43] B. I. Choi, "Radiative Substrate Heating for High-Tc Superconducting Thin-Film Deposition," *J. Vac. Sci. Technol.*, vol. 10, p. 3407, 1992.

[44] J. A. Thornton, "The Influence of Bias Sputter Parameters on Copper Coating," *Thin Solid Films*, vol. 40, p. 337, 1977.

[45] J .A. Thornton, "Residual Stresses in Sputtered Ti Films," *J. Vac. Sci.*, vol. 12, p. 833, 1975.

[46] J. A. Thornton, "The Influence of Bias Sputter Parameters on Copper Coating," *Thin Solid Films*, vol. 40, p. 334, 1977.

[47] D. W. Hoffman and J. A. Thornton, "Residual Stresses in Metal Films," *Thin Solid Films*, vol. 40, p. 335, 1977.

[48] S. Inove and N. Ishika, "Effect of Si:Ta Ratio on Sputter Deposition of Silicides," *J. Electrochem. Soc.*, vol. 128, p. 2405, 1981.

[49] R. Honig, "Properties of Magnetron Sputtering," *J. Appl. Phys.*, vol. 29, p. 552, 1985.

[50] M. E. Hilley and R. E. Rickefs, "Residual Stress Measurement by X-ray Diffraction," *SAE information Report*, p. 786, 1971.

[51] H. Ljungcrantz, L. Hultman and J. E. Sundgren, "Residual Stresses and Fracture Properties of Magnetron Sputtered Ti Films," *J. Vac. Sci. Technol.*, A11(3), p. 556, 1993.